PHYSICAL REVIEW D **110,** 092011 (2024)

First measurement of the total inelastic cross section of positively charged kaons on argon at energies between 5.0 and 7.5 GeV

A. Abed Abud *et al.*[*]
(DUNE Collaboration)

(Received 2 August 2024; accepted 20 September 2024; published 14 November 2024)

ProtoDUNE Single-Phase (ProtoDUNE-SP) is a 770-ton liquid argon time projection chamber that operated in a hadron test beam at the CERN Neutrino Platform in 2018. We present a measurement of the total inelastic cross section of charged kaons on argon as a function of kaon energy using 6 and 7 GeV/c beam momentum settings. The flux-weighted average of the extracted inelastic cross section at each beam momentum setting was measured to be 380 ± 26 mbarns for the 6 GeV/c setting and 379 ± 35 mbarns for the 7 GeV/c setting.

DOI: 10.1103/PhysRevD.110.092011

I. INTRODUCTION

Liquid argon time projection chambers (LArTPCs) may be used to measure the trajectories of charged particles with millimeter resolution. This capability makes the detectors, like those of the Deep Underground Neutrino Experiment (DUNE) far detector modules, sensitive to studying GeV-scale and MeV-scale neutrinos and searching for physics beyond the Standard Model [1]. An example of important physics that can be done using the DUNE far detector modules is a search for proton decay to a final state with a neutrino and a charged kaon ($p \to \nu + K^+$), which is predicted to be dominant in a broad class of supersymmetric grand unified theories [2–6]. Unlike searches in water Cherenkov detectors [7], DUNE can detect the final-state kaon, which has a momentum of 330 MeV/c absent final-state interactions. The efficiency of observing this signature is sensitive to modeling kaon transport in the LAr medium, which is limited by the dearth of kaon-argon scattering data. This search for nucleon decay requires a representative model of kaon transport and interactions in liquid argon to ensure an accurate simulation of signal events. Without reliable data and simulations, the relevant uncertainties for the kaon cross section on argon cannot be constrained. This can lead to large systematic uncertainties in nucleon decay searches with a potentially biased cross-section model.

As a first step toward collecting high-quality kaon-argon interaction data, the ProtoDUNE Single-Phase (ProtoDUNE-SP) large-scale prototype of a DUNE far detector module was exposed to a test beam from the H4-VLE beamline at CERN that included kaons at 6 and 7 GeV/c [8,9]. ProtoDUNE-SP is a 770-ton LArTPC with the same drift distance and full-scale engineering parts as a DUNE Far Detector Horizontal Drift module. It measures the tracking and calorimetry of charged particles by detecting the ionization electrons that drift toward three layers of wire planes. The H4-VLE beamline, a tertiary beam from the CERN Super Proton Synchrotron, is referred to as simply the "beam" in many places in this paper. ProtoDUNE-SP collected data from the beam, using many beamline momentum settings, over two months from September 2018 to November 2018.

The data from ProtoDUNE-SP can be used by event generators that simulate hadron-nucleus interactions, like the neutrino event generator GENIE [10–14] and the transport and interaction simulation program GEANT4 [15–17], to improve the modeling of kaon interactions on argon nuclei. The kaon-argon cross section has never been measured as a function of energy on argon. Therefore, the purpose of this analysis is to provide the first measurement of the total inelastic cross section of kaons on argon at these high energies. Neither GENIE nor GEANT4 has recommended uncertainties for kaon-argon interactions, providing a unique opportunity for ProtoDUNE-SP to inform inputs on associated modeling uncertainties.

In this work, the kaon-argon total inelastic cross section is reported as a function of kaon energy within the limits of the detection threshold, described in Sec. IV. Figure 1 shows the total inelastic and the elastic cross section predicted by the GEANT4 Bertini cascade model [15–17]. Charged kaons produced by the beam with kinetic energies of approximately 4.5 to 7 GeV are capable of reaching the liquid argon of ProtoDUNE-SP. Using the GEANT4 prediction from Fig. 1, the simulated total inelastic cross

---

[*] Full author list given at the end of the article.

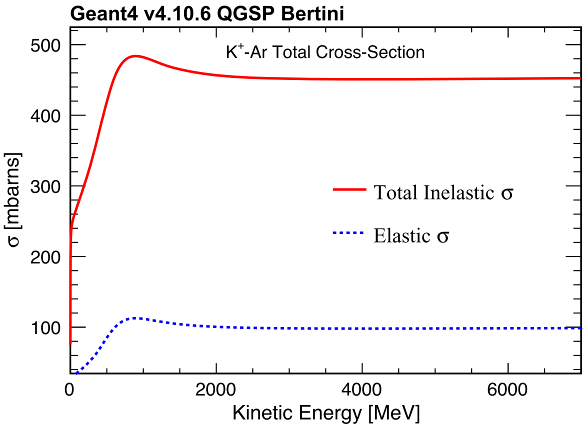

FIG. 1. GEANT4 predicted total inelastic cross section and elastic cross section of positively charged kaons on argon as a function of kinetic energy [15–17]. Predictions made using interfaces in Ref. [18].

section at the relevant energies should be approximately 450 millibarns (mbarns).

Section II discusses ProtoDUNE-SP more broadly, and Sec. III outlines the simulation and reconstruction of ProtoDUNE-SP data. Section IV explains the *thin slice method* used in this measurement. This method divides the detector into thin targets, referred to as *thin slices*, using the wires of the LArTPC to demarcate the slices. An *incident* slice is counted if a particle reaches a particular wire. Within that slice, it may also interact on the argon, which means the slice contains both an incident and an *interacting* slice. After an interacting slice is detected, the counting for the event stops as the outgoing particles have unknown identities and energies. The cross section is measured using the counts of the incident and interacting slices as a function of kinetic energy.

Section V describes the selection of candidate kaon interaction events, and Sec. VI shows energy-related measurements using selected kaons. Section VII reports the kaon-argon cross section with comparisons to models. Section VIII discusses the evaluations of the statistical and systematic uncertainties.

II. PROTODUNE-SP AND THE H4-VLE BEAMLINE

ProtoDUNE-SP is a 770-ton liquid argon detector that is 7.2 m wide, 6.1 m high, and 7 m long. It has two TPCs, each with a drift distance of 3.6 m [9]. The detector contains six readout wire planes called anode plane assemblies (APAs), with three APAs for each drift volume. Each APA contains three readout wire planes—the U, V, and X wire planes—and are 6.2 m high, 2.3 m long, and 0.1 m thick [9]. The U and V wires are the first two planes and detect drifting electrons via the currents induced on the wires as the charges drift past them, creating bipolar signals. The X wires, known as collection wires, have unipolar signals where the drifting electrons collect on the wires and stop drifting in the TPC [9]. The U, V, and X wires are oriented 35.7°, −35.7°, and 0° relative to the vertical direction, respectively. The pitch between wires is 0.467 cm for induction wires and 0.479 cm for collection wires. Each APA has 960 X wires, 800 U wires, and 800 V wires.

Three APAs are installed in a 7 m line and sit in front of one sidewall of the cryostat, and the other three APAs are installed in a similar fashion in front of the opposite sidewall of the cryostat. These APAs are 7.2 m away from each other, and the cathode plane assembly (CPA) sits midway between the two separate walls of APAs. The CPA provides a high voltage of 180 kV, leading to a nominal electric field strength of 500 V/cm across the 3.6 m separating each APA from the CPA, which allows the ionization electrons to drift to the APAs. The H4-VLE beam pipe connects to the upstream face of LArTPC via a low-density beam plug that allows the beam to enter without scattering off the material in the cryostat [8,9].

The beam only enters one TPC of the detector. The beam side of the detector has the vertical gap between APAs instrumented with electron diverters that intend to improve charge-collection efficiency for electrons drifting near the gap between neighboring APAs. Unfortunately, these electron diverters exhibited high-voltage shorts and were left electrically grounded during operations, distorting the track images and causing some loss of collected charge.

As a surface-based detector, ProtoDUNE-SP is exposed to an intense flux of cosmic-ray muons, which create electron-ion pairs in the detector. The argon ions drift slower than the ionization electrons, leading to an excess of ions around the surface of the detector. The excess of ions creates a space charge effect that alters the local electric field, leading to distorted calorimetry and tracking [19].

A calibration of the space charge effect is completed by measuring the tracking distortions on the surfaces of the detector, where the effect is maximal, with cosmic-ray muon data [8]. The distortions measured are then used to correct for local electric field fluctuations by using a linearly interpolated three-dimensional map. An “inverted” map using these data measurements is used to recreate the space charge effect in simulation. The original three-dimensional map is utilized to calibrate this effect in simulation.

From September 2018 to early November 2018, the H4-VLE beamline settings were adjusted to emit positively charged particles at 0.3, 0.5, 1, 2, 3, 6, and 7 GeV/*c* beamline momentum settings. The beamline trigger operates at a rate of 25 Hz, which qualitatively translates to beam particles being observed one at a time within ProtoDUNE-SP. The beam consists of positively charged protons, positrons, kaons, pions, and muons. The beam particle species is identified using a time-of-flight system and Cherenkov detectors. The beam particle momentum is measured from the bend of the particle’s trajectory through a well-known magnetic field using data from tracking fibers [8,20]. The 6 GeV/c and 7 GeV/c beam momentum settings are the only settings that produce kaons that reach ProtoDUNE-SP. The kaons are identified using only the Cherenkov detectors, explicitly requiring a signal in the high-pressure Cherenkov detector but no signal in the low-pressure Cherenkov detector [8].

III. SIMULATION AND RECONSTRUCTION

A simulation of the beam, including its transport to and through the LArTPC, is implemented using GEANT4 [15–17], with the entire CERN H4-VLE facility simulated from the primary beam to the tertiary beam that reaches ProtoDUNE-SP [20]. The selection of kaon inelastic scattering events starts with the beamline instrumentation discussed in Sec. II. A kaon event is defined as any time the beamline instrumentation has a signal recorded by the high-pressure Cherenkov detector and the absence of a signal recorded by the low-pressure Cherenkov detector [8].

The rest of the selection steps rely on information from the reconstruction of tracks and showers in the TPC to select relevant events. Additionally, the beamline instrumentation also has tracking fibers to reconstruct a beam track that can be extrapolated to the TPC [8,20]. These steps will be described in Sec. V.

ProtoDUNE-SP uses the Pandora multialgorithm reconstruction package to identify the beam particle, reconstructing particle hierarchies using pattern recognition [8,21,22]. It then employs a boosted decision tree to select beam particle candidates that enter through the beam pipe and beam plug into the liquid argon detector. A full description of the software used in ProtoDUNE-SP is given in Refs. [8,22].

Figure 2 shows the observed and simulated distributions of the reconstructed track lengths for events with a beam kaon, as determined by the beamline instrumentation, for the 6 GeV/c samples. The corresponding distributions for the reconstructed track lengths and all other event selection distributions for the 7 GeV/c samples showed similar agreement and are included in the Appendix. The spikes in Fig. 2 at around 230 cm and 460 cm correspond to broken tracks caused by the electron diverters that sit in the gaps between the APAs, as discussed in the previous section, with the last spike at around 700 cm corresponding to the end of the active volume. Most TPC tracks are secondary particles without any TPC-related selection steps. An excess of short reconstructed track lengths is observed in the data, likely driven by background secondary particles.

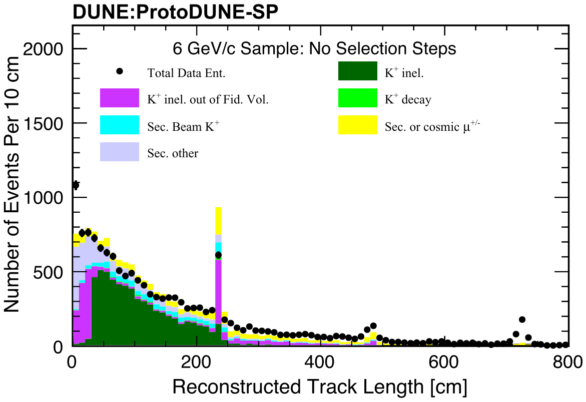

FIG. 2. Reconstructed track length for simulation and data without any TPC-related selection steps at the 6 GeV/c beamline setting. Events in simulation are classified by the true identities and fates of the reconstructed TPC tracks, including secondary particles (sec.) from kaon interactions that are misidentified as the beam particle. Only statistical uncertainties from the statistics in data are shown. The statistics of the simulation are scaled to match the normalization of all data events, including those without a reconstructed track in the TPC.

The interaction point—or track endpoint—is determined using clustering and vertex-finding algorithms that are almost identical to those from the MicroBooNE reconstruction and are described in detail in Ref. [23]. The initial clustering aims to make small clusters that contain energy depositions from a single particle and avoid erroneously clustering energy from multiple particles into a single cluster. Numerous algorithms then associate these pure clusters together, aiming to produce a single cluster containing all energy depositions from a single particle. In addition, algorithms are applied to split clusters if kinks are found or where the topology suggests that there may be contributions from multiple particles. These clusters are classified as either tracks or showers based on their topologies. Candidate 3D interaction points are produced by comparing pairs of clusters from two 2D views and reconstructing their start and end points as candidate interaction points. Pandora uses a boosted decision tree to select the vertex candidate most likely to correspond to the interaction point of the beam particle. The signal process is an inelastic interaction of the incident kaon. An inelastic interaction in this analysis is defined as any process where either:

(i) the angle between the beam kaon and leading outgoing particle is greater than 11 degrees

(ii) two or more particles emerge from the interaction point.

The kinetic energy threshold for observing a final-state proton or charged kaon in the detector is 40 MeV, and for a charged pion it is 20 MeV. We apply these restrictions to our signal definition.

IV. METHODOLOGY

The cross-section measurements presented in this paper use the *thin slice method* pioneered by the LArIAT experiment [24,25]. The approach treats the detector as a series of thin argon targets (slices). The number of surviving particles (N_{surv}) is:

$$N_{\mathrm{surv}}(d) = N_{\mathrm{inc}} \exp(-d/l) = N_{\mathrm{inc}} \exp(-\sigma d n), \quad (1)$$

where N_{inc} is the number of incident particles, d is the distance traveled, and $l = (n\sigma)^{-1}$ is the interaction length of a kaon in argon, where n is the number density and σ is the cross section.

A natural way to develop slices in a LArTPC with a wire readout is to use the individual wires to demarcate thin target slices from one another. Therefore, a slice is a three-dimensional box of argon between wires. For each particle, the incident energy at each thin slice is estimated. The total number of particles at each incident energy (N_{inc}) is counted, as are the total number of interactions (N_{int}). Regardless of whether or not there was an interaction, if an energy deposit from the kaon is registered in a thin target slice, then the slice is counted in the bin corresponding to the kinetic energy of the kaon in that slice (N_{inc}). The cross section, using Eq. (1), is:

$$\sigma(E_{\mathrm{kin}}) = \frac{M_{\mathrm{Ar}}}{N_{\mathrm{A}} r \rho} \ln\left[\frac{N_{\mathrm{inc}}(E_{\mathrm{kin}})}{N_{\mathrm{inc}}(E_{\mathrm{kin}}) - N_{\mathrm{int}}(E_{\mathrm{kin}})}\right], \quad (2)$$

where E_{kin} is the kinetic energy of the particle, N_{A} is the Avogadro constant, M_{Ar} is the atomic mass of argon, ρ is the density of liquid argon, and r is the three-dimensional distance the particle travels from one wire to the next [24,25]. The value of r is 0.498 cm, given the wire spacing between the collection plane wires of 0.479 cm and that the beam travels at a 16-degree angle in the detector.

The kinetic energy at a given slice ($E_{\mathrm{kin,j}}$) is reconstructed as:

$$E_{\mathrm{kin,j}} = E_{\mathrm{kin,beam}} - \sum_{i=0}^{j-1} \Delta E_i, \quad (3)$$

where $E_{\mathrm{kin,beam}}$ is the initial beam particle kinetic energy and ΔE_i is the measured energy lost in slice i. The total ΔE is summed from all slices up to slice j.

Background subtractions, unsmearing, and efficiency corrections are required to convert the measured interaction and incident spectra into a cross section. These corrections are applied via RooUnfold with unfolding done using a Bayesianlike unfolding algorithm implemented based on Richardson-Lucy deconvolution [26–30]. The process includes background subtraction, unsmearing, and efficiency corrections. These corrections are applied on the incident and interacting slice distributions separately, an approach similar to that previously used by LArIAT [25]. These unfolded distributions of the incident and interacting slices are then used in Eq. (2) to measure the cross section as a function of kinetic energy.

V. EVENT SELECTION

There are three event selection steps to select candidate kaons and an additional step to select a candidate kaon with an inelastic interaction. They include the following selection steps for events where the beamline trigger reports a kaon candidate:

(i) the event must have a reconstructed TPC track.
(ii) the endpoint of the TPC track must enter the fiducial volume by being at least 30 cm downstream of the start of the active volume of the detector. This selection step is motivated by significant inefficiencies and impurities in correctly identifying and reconstructing the beam particle with a TPC track in the first 30 cm of the detector.
(iii) the TPC track must be matched to the trajectory of the beam track from the beamline instrumentation. A match requires that their positions and angles agree within three times the standard deviations of the distributions for these measurements at the start of the fiducial volume.

Because the electron diverters tend to break tracks, as discussed in Sec. II, only the interaction and incident slices contained before the point of 220 cm across the detector length, which corresponds to collection plane wire 464, are considered in the cross section measurement. This is the final step. At each collection wire, the kaon energy is estimated per Eq. (3), and the kaon either undergoes an interaction or does not. Thus, for each incident particle, we observe many "slices" and record the interaction as a function of energy. The interaction point—or vertex—identification occurs through Pandora as described in Sec. III. Event displays of some selected kaon inelastic interaction candidates are shown in Fig. 3. In these events, the beam enters the TPC at time tick 4750, where a time tick represents the 500 ns sampling intervals of the analog-to-digital converters for the wires, and then it travels over 50 cm before interacting with the argon. The beam particles, highlighted by the black ovals, travel in approximately straight lines from the left to the right before scattering, creating complicated final states with many showers. The top two event displays show little shower activity, indicating they may be candidate events with a final state with one positively charged kaon and other nonstrange hadrons. The third event display shows a complex interaction with many showers and tracks in the final state.

Figure 4 shows the distributions of reconstructed track lengths for selected TPC tracks that will form the incident and interacting slice spectra from the 6 GeV/c beamline setting. Secondary kaons, which are byproducts of true beam kaons interacting off the argon and traveling with some unknown kinetic energies, are the most significant background for the event selection. As these secondary kaons will have similar characteristics to beam kaons, they

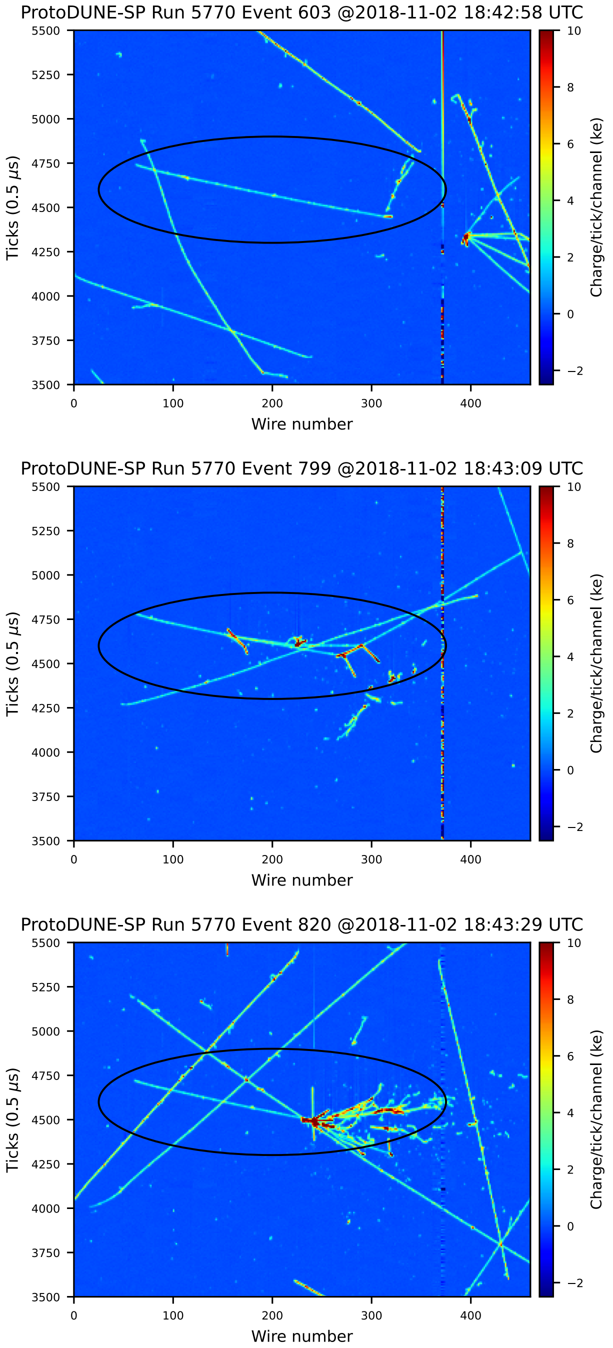

FIG. 3. Three candidate event displays of selected beam kaons, highlighted in black, that inelastically interact on the argon from data taken in early November 2018. The beam travels from the left to the right at an angle of approximately 16 degrees. Cosmic-ray muons can be seen in the foreground and background of the beam event, and a nonfunctioning wire can be observed near wire 370.

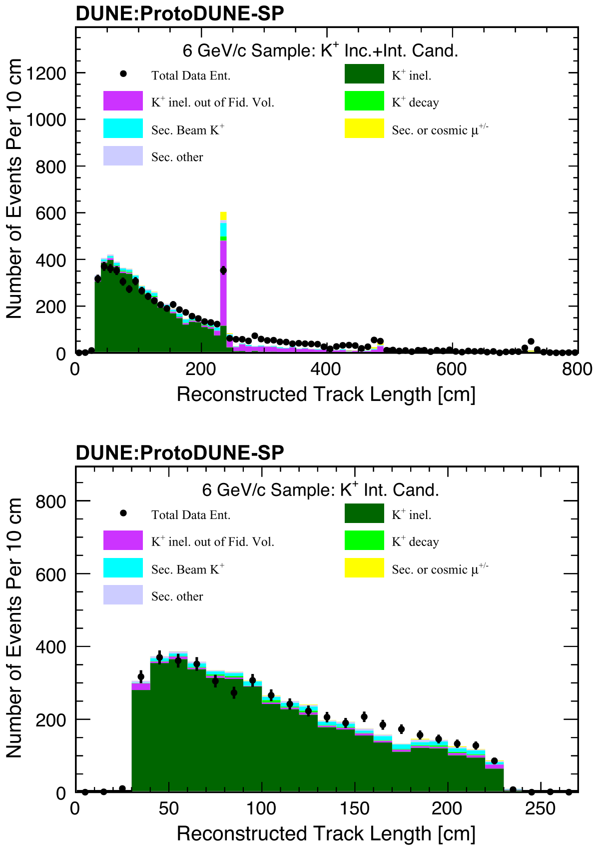

FIG. 4. Reconstructed track length for simulation and data of the 6 GeV$/c$ beamline setting for selected kaons (top) and for selected kaons that interact within the fiducial volume (bottom). Only statistical uncertainties are shown for the data, and the statistics from the simulation are scaled to match those from the data.

are an irreducible background. The breakdown of the data and simulation samples through each selection step are shown in Table I.

The selection efficiency and purity are evaluated as a function of kinetic energy from simulation. An inefficiency in measuring a slice of kinetic energy occurs when no TPC track corresponds to the beam particle in the slice. A background slice occurs when there is a TPC track in a slice that the true kaon does not reach. The definition for a background slice is used regardless of whether the TPC track is from a true kaon or not, which allows the analysis to fully recover the truth-level distributions when unfolding reconstruction information taken from the nominal simulation. Results are shown in Fig. 5. The purity is close to 95% for interacting slices and 85% for incident slices. The lower purity is because a single background particle entering the detector contributes to many noninteracting slices, but only a single inelastic interaction can occur per particle. The efficiency varies between 35 and 40% as a function of energy. The inefficiencies are dominated by events with a true kaon in the fiducial volume, but the event did not have a TPC track identified as the beam particle.

VI. ENERGY MEASUREMENTS AND BINNING

As referenced in Eq. (3), the initial kinetic energy is determined using measurements from the beamline

TABLE I. Information on the fractions of the samples remaining for data and simulation after each selection step from the left (beamline reports a candidate kaon) to the right (candidate kaon has an interaction in the fiducial volume). In this table, a beam kaon with an inelastic interaction in the fiducial volume is defined as a signal event.

Selection step	Beam (%)	TPC track (%)	Fiducial (%)	Beam-TPC match (%)	Contained interaction (%)
6 GeV/c data	100.0	58.0	46.0	25.4	18.6
7 GeV/c data	100.0	55.6	44.8	27.3	19.5
6 GeV/c sim total	100.0	55.0	44.7	29.1	23.2
6 GeV/c sim signal	24.9	24.4	24.0	21.8	20.9
6 GeV/c sim bkg	75.1	30.6	20.7	7.3	2.2
7 GeV/c sim total	100.0	45.1	36.5	24.0	19.1
7 GeV/c sim signal	20.9	20.4	20.0	18.3	17.5
7 GeV/c sim bkg	79.1	24.7	16.5	5.6	1.5

instrumentation. Figure 6 displays the beamline kinetic energy measurements of the selected beam kaons. The impact of the systematic uncertainty is found by shifting the data distribution by the 1.2% kinetic energy modeling uncertainty of the beamline simulation, which will be discussed in greater detail in Sec. VIII.

The TPC calorimetry is calibrated by applying corrections to the electric field variations, corrections for the spatial variations, and an overall charge scale using through-going and stopping cosmic-ray muons [8]. The energy resolution was evaluated and done by measuring the difference between the true and reconstructed kinetic energies at the interaction points in the simulation. The minimum resolution is measured to be 124 MeV, as seen in Fig. 7.

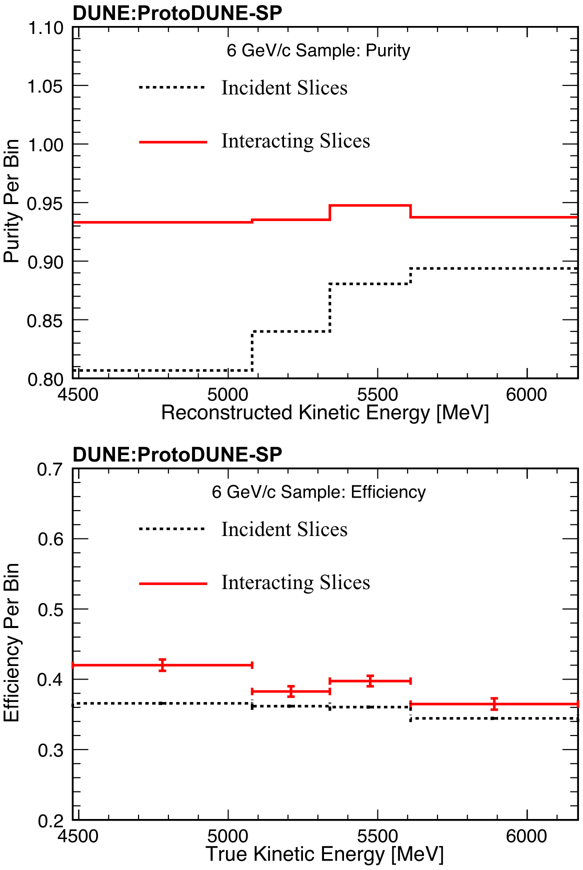

FIG. 5. Purity (top) and efficiency (bottom) of the event selection for each bin for the 6 GeV/c simulation sample.

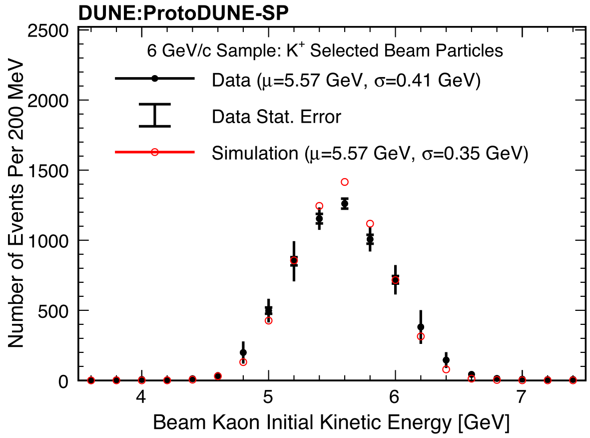

FIG. 6. Initial beam particle kinetic energy as measured by the beamline instrumentation for selected kaon candidate tracks for the 6 GeV/c beamline setting. Both systematic and statistical uncertainties are shown.

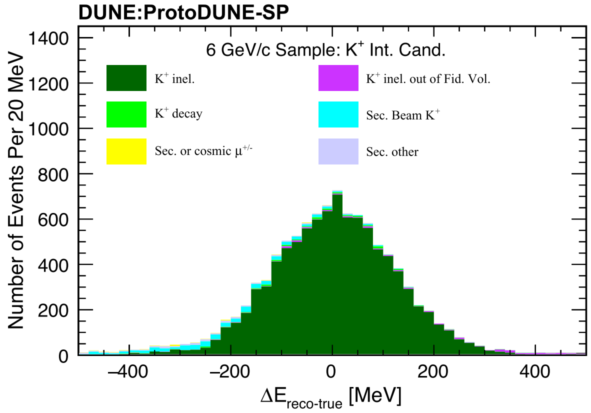

FIG. 7. Kinetic energy resolution at the interaction point of beam particles that pass all selection criteria for interacting kaons in the 6 GeV/c simulation sample. The distribution has a mean energy bias of 0.50 MeV. The distribution is not scaled to the statistics in the data.

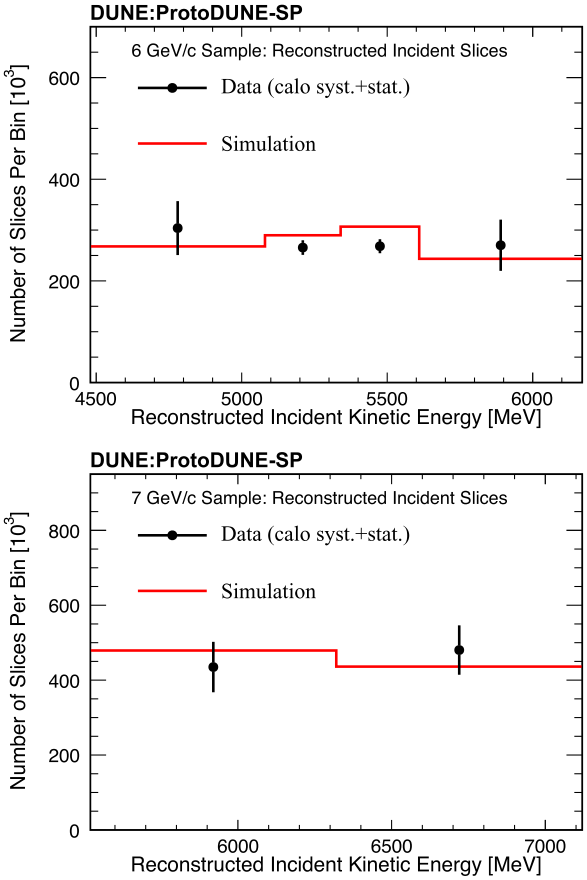

FIG. 8. Reconstructed incident slice distributions between the data and simulation for the 6 GeV/c beamline setting (top) and the 7 GeV/c beamline setting (bottom). A calorimetric slice-by-slice uncertainty of 3% and a beam kinetic energy scale uncertainty of 1.2% are applied to the data. Statistics for the simulation are scaled to match the normalization from the data.

However, there are systematic uncertainties associated with the simulation of the detector response and limited statistics, making this not the definitive resolution. For example, there is a 3% uncertainty on the calorimetry calibration and a 1.2% uncertainty on the beam momentum measurement, which corresponds to a maximum energy discrepancy of approximately 80 MeV. The binning of the analysis ensures equal statistics in each bin for the reconstructed interacting slice distributions in the data sample for both beam momentum settings. The minimum bin size is then 260 MeV, which is greater than the resolution measured in simulation and the uncertainties from calorimetry.

The reconstructed slice distributions, highlighting both the binning and slice distributions as a function of energy, are shown for incident slices in Fig. 8 and for interacting slices in Fig. 9. Calorimetric-related uncertainties, fully discussed in Sec. VIII, are applied to these distributions.

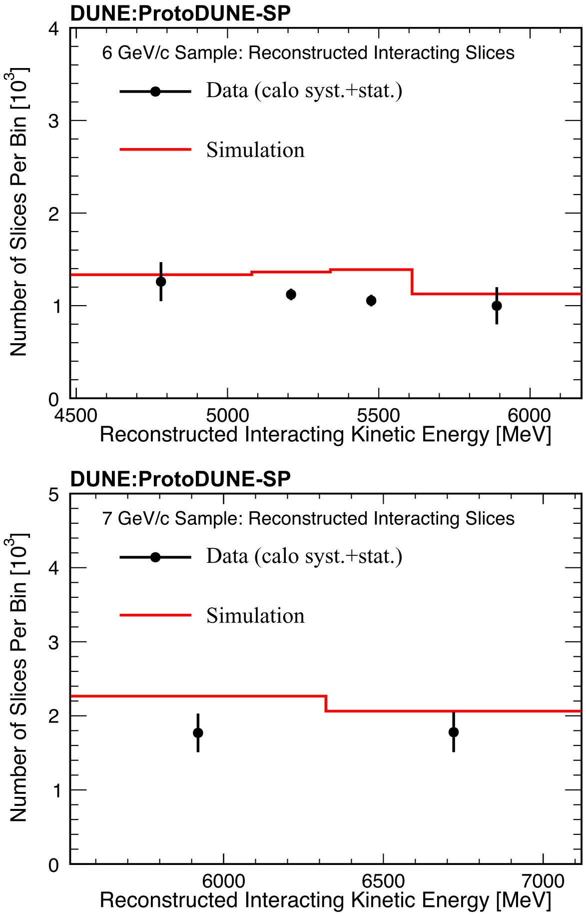

FIG. 9. Reconstructed interacting slice distributions between the data and simulation for the 6 GeV/c sample (top) and the 7 GeV/c sample (bottom). A calorimetric slice-by-slice uncertainty of 3% and a beam kinetic energy scale uncertainty of 1.2% are applied to the data. Statistics for the simulation are scaled to match the normalization of incident slices from the data.

VII. RESULTS

The kinetic energy distributions for all kaons—and for interacting kaons—are separately unfolded using the method of D'Agostini with four iterations [26–29]. The smearing matrices are shown in Figs. 10 and 11. Studies were done to test unfolding by altering the regularization, not correcting for bin-to-bin smearing, and changing the background subtraction and efficiency corrections. All had an impact of less than a percent on the average cross section compared to the nominal unfolding process described above. The response matrix is obtained using only 66% of the simulated data, which was done to use the remaining 33% as statistically independent fake data samples for investigating systematic uncertainties.

The reconstructed slice spectra, shown in Figs. 8 and 9, are unfolded and then used to measure the cross section with Eq. (2) with uncertainties that will be described in Sec. VIII. Figure 12 displays the result for the data of the

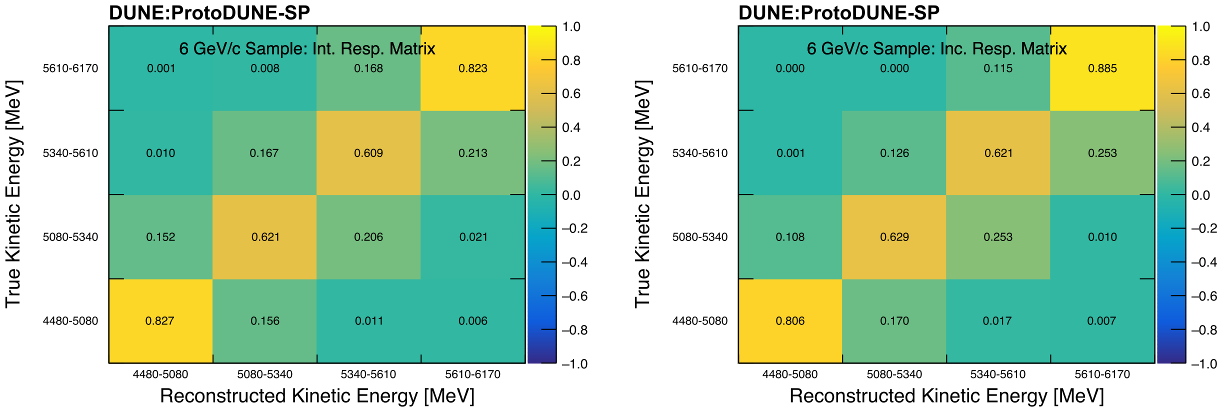

FIG. 10. Response matrices for the 6 GeV/c simulation sample of the interacting (left) and incident (right) spectra. The entries in the matrices are normalized so that the rows sum to one.

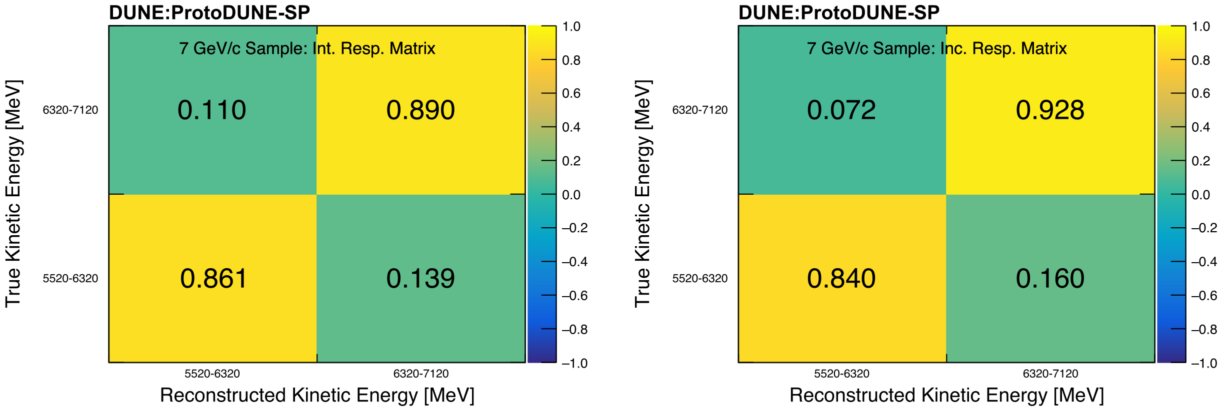

FIG. 11. Response matrices for the 7 GeV/c simulation sample of the interacting (left) and incident (right) spectra. The entries in the matrices are normalized so that the rows sum to one.

6 GeV/c sample with comparisons to predicted cross sections from GEANT4, GENIEv3.2.0 hA2018, and GENIEv3.2.0 hN2018 [10–12,14–17,31]. GENIE calculates the total cross section using data and partial wave analysis [32]. It simulates interactions with either an empirical model (hA2018) or a fully simulated cascade (hN2018) [11,14]. GEANT4 applies alterations of the base model cross section using data sets included in the Particle Data Group

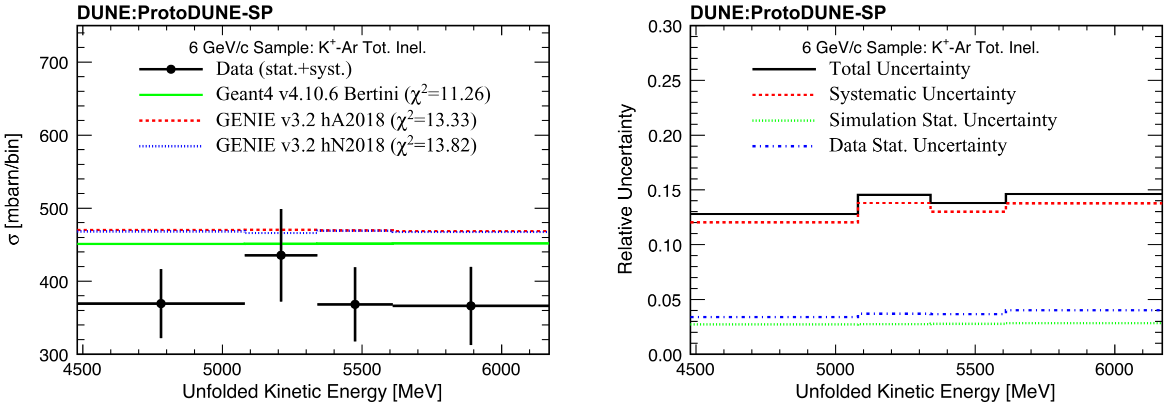

FIG. 12. Extracted total inelastic cross section from beam kaons at the momentum setting of 6 GeV/c (left) with comparisons to GENIEv3.2.0 and GEANT4 [10–12,14–17,31]. The relative uncertainties of the measurements are also shown (right). The hA2018 and hN2018 cascade simulations of GENIE provide nearly the same prediction, and their distributions overlap.

TABLE II. Total inelastic positively charged kaon cross section with uncertainties for data from the 6 GeV/c momentum setting beam. The total uncertainties (δ_{tot}) are broken down into the systematic uncertainty (δ_{syst}), statistical uncertainty from limited data statistics ($\delta_{\mathrm{stat}}^{\mathrm{Data}}$), and statistical uncertainty from limited simulation statistics ($\delta_{\mathrm{stat}}^{\mathrm{Sim}}$). All units for the cross section and uncertainties are in millibarns.

Energy bin (MeV)	σ_{inel} (mbarns)	δ_{tot}	δ_{syst}	$\delta_{\mathrm{stat}}^{\mathrm{Data}}$	$\delta_{\mathrm{stat}}^{\mathrm{Sim}}$
4480–5080	369	47	44	13	10
5080–5340	435	63	60	16	12
5340–5610	368	51	48	13	10
5610–6170	366	54	50	15	10

summary cross-section measurements [33]. The reduced chi-squared statistics between these models over four bins are 11.26 for GEANT4 and 13.33 for GENIEv3.2.0 hA2018. The 6 GeV/c data sample flux-averaged cross section is measured at 380 ± 26 mbarns. Table II shows the final results with the breakdown of the uncertainties applied.

Figure 13 presents the cross section measured with data at the 7 GeV/c beam setting. The reduced chi-square statistic measured divided by the number of bins is 2.64/2 bins for GEANT4 and 4.05/2 bins for GENIEv3.2 hA2018. Table III displays the final result with uncertainties broken down by category. The flux-averaged cross section is 379 ± 35 mbarns for the 7 GeV/c sample. Encouragingly, the bin whose energy range overlaps with the 6 GeV/c sample has a similar measured cross section, which is within uncertainties.

VIII. TREATMENT OF UNCERTAINTIES

Uncertainties are propagated by randomly sampling statistical and systematic parameters 1000 times within their *a priori* uncertainties [34]. The impact of the statistical uncertainty on the individual kinetic energy bins of the incident and interaction spectra is assessed by randomly Poisson-fluctuating the number of entries in each bin independently according to the measured counts. It is done this way as the statistical uncertainty of the cross section is not directly proportional to the statistical uncertainty of interaction points given that the interaction and incident distributions are inside a logarithm, as seen in Eq. (2). However, there are enough statistics in the incident and interacting distributions to assume both are Poisson-distributed and uncorrelated; therefore, doing many independent fluctuations of each bin can acquire the statistical uncertainty on the cross section by remeasuring the cross section with each Poisson-fluctuated sample. The resulting uncertainty on the measured cross section is approximately 2.7%, as shown in Tables II and III.

TABLE III. Total inelastic positively charged kaon cross section with uncertainties for data from the 7 GeV/c momentum setting beam. The total uncertainties (δ_{tot}) are broken down into the systematic uncertainty (δ_{syst}), statistical uncertainty from limited data statistics ($\delta_{\mathrm{stat}}^{\mathrm{Data}}$), and statistical uncertainty from limited simulation statistics ($\delta_{\mathrm{stat}}^{\mathrm{Sim}}$). All units for the cross section and uncertainties are in millibarns.

Energy bin (MeV)	σ_{inel} (mbarns)	δ_{tot}	δ_{syst}	$\delta_{\mathrm{stat}}^{\mathrm{Data}}$	$\delta_{\mathrm{stat}}^{\mathrm{Sim}}$
5520–6320	386	42	38	11	15
6320–7120	367	61	59	10	14

The finite statistics of the simulation sample primarily impact the analysis via the background subtraction, unsmearing, and efficiency corrections. This effect is propagated by varying the number of counts in each kinetic energy bin for the backgrounds, inefficiencies, and within the response matrix. Values from sampling a Poisson distribution are used to regenerate the response matrices

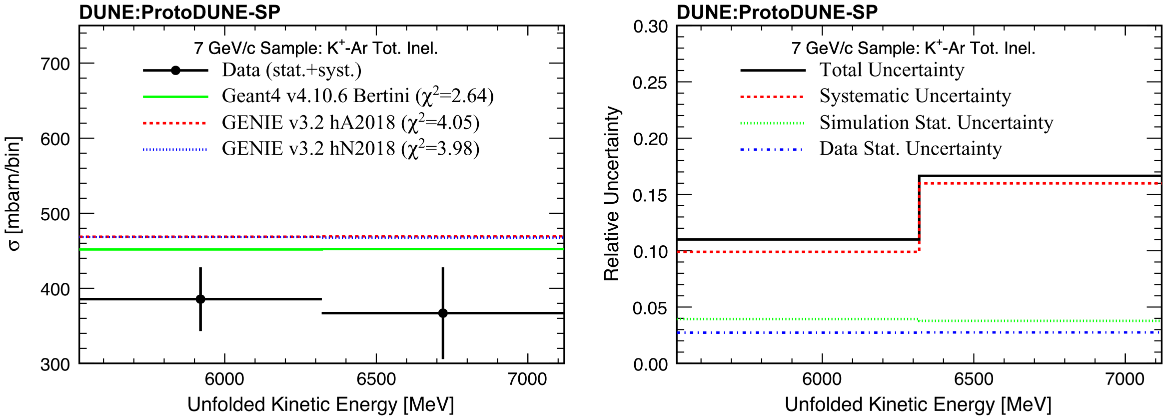

FIG. 13. Extracted total inelastic cross section from beam kaons at the momentum setting of 7 GeV/c (left) with comparisons to GENIEv3.2.0 and GEANT4 [10–12,14–17,31]. The relative uncertainties of the measurements are also shown (right). The hA2018 and hN2018 cascade simulations of GENIE provide nearly the same prediction, and their distributions overlap.

and affiliated corrections, with each bin treated as independent from the others. As statistics in the incident slices are significantly larger than those of the interacting slices, by a factor of around 200 as shown in Fig. 8, this uncertainty is only applied to the response matrix and affiliated corrections for interacting slices.

The systematic uncertainties considered in this analysis are related to the simulation of the beamline and beamline instrumentation, the TPC response, the hadron transport model, and instances in which modeling and reconstruction of the TPC data are ill-posed. The results from unfolding with the new response matrices are used to address the total impact of the systematic effects on the analysis.

The systematic term associated with the beamline momentum scale arises from uncertainties in terms of the position of the fiber monitors and the magnetic field strength in the beamline instrumentation. This value was calculated as 1.2% [35] of the beam particle energy. Therefore, the energy of the beam kaon is fluctuated according to a Gaussian distribution with width of 1.2%, resulting in an approximately 2% uncertainty on the measured cross section.

Furthermore, the particle itself can "scrape" against material upon entering the liquid argon, losing energy in the process. These beam "scrapers" should appear in selections if their position is greater than 1.5 times the radius of the beam away from the beam center (r_{beam}). There are 3.15 times more selected events in data that exceed this $1.5r_{\mathrm{beam}}$ metric than in simulation. Therefore, the systematic uncertainty treatment alters the frequency of the beam "scrapers" with a central value weight of 3.15 and a standard deviation of 2.15 to address the difference between data and simulation. The weight upscales simulation events whereby the beamline instrumentation system momentum and truth information momentum at the TPC differ by over 200 MeV, the estimated minimal energy lost for a beam "scraper."

A 3% calorimetric uncertainty from the TPC is assumed in the energy determination. This value is taken from evaluations of the calorimetry calibration uncertainty [36]. That study observed the spread in charge calibration results from subsamples of cosmic-ray muons separated by their trajectories in the detector, based on a similar analysis from MicroBooNE [37]. Although the ProtoDUNE-SP study measured 2% deviations in calibration values, a 3% uncertainty is applied to address time-dependent fluctuations in the spread of calibration results.

The space charge effect, as discussed in Sec. II, may alter the reconstructed positions of particles. The fiducial volume is defined to reduce the impact of the space charge effect on the track reconstruction efficiency. Mismodeling of the space charge distribution in the TPC can be effectively treated as shifts in the boundaries of the fiducial volume. The impact of the uncertainty of the space charge modeling is estimated using the spread in the mean distortion at the surfaces of the detector over time. The uncertainty on the spatial distortions from the space charge effect was measured to be 8%.

The systematic uncertainty in this analysis arising from mismodeling of charged kaon scattering is assessed by using the GEANT4REWEIGHT package [18] to reweight events based on the total signal cross section, which intends to probe how the underlying simulated cross section impacts the background subtraction and efficiency corrections. The total inelastic cross section was varied by 20%. Additionally, differences in vertexing due to the multiplicities and charges of kaons in the final state were observed in the simulation. Therefore, the number of interactions with one positively charged kaon and any number of nonstrange hadrons in the final state, one of the two dominant exclusive channels, is reweighted by 20%. The weighting is done in a manner to hold the total cross section constant. The other dominant channel, which occurs as frequently, is a final state with a single neutral kaon and any number of nonstrange hadrons. The impact of all these modeling uncertainties is 2–6% on the cross section per bin.

The impact of mismodeling the effect of the electron diverter is determined by changing the frequency of these events occurring in the incident response matrices. The following uncertainty increases and decreases the relative number of tracks broken by the electron diverters. It only applies to tracks that do not end within the fiducial volume, which means this weight only impacts the incident slice spectrum. The uncertainty on this effect is set to 100%, as the rate at which the electron diverter breaks reconstructed tracks is not well simulated and overpredicts the number of broken tracks, as seen in Fig. 2.

While Pandora employs various algorithms to find the end point of the beam particle, they may miss the vertex, as Fig. 14 shows that the endpoint of the reconstructed track may not exactly be the true endpoint. These events may still have kaon inelastic scatters in the fiducial volume. However, these events may underestimate or overestimate the number of incident slices of the beam particle, biasing the results. These tracks are called either broken or extended tracks. An additional uncertainty term was introduced to address the miscounting of incident slices from inaccurate vertex positions, changing the "flux" in a *thin slice* measurement. The uncertainty changes the relative frequency of kaons in simulation with reconstructed vertices that are more than 5 cm away from the true interaction vertices. A 100% uncertainty on their frequencies in simulation is assumed for both broken and extended tracks, as data-driven constraints cannot be provided on vertexing.

The fiducial volume is chosen to minimize the impact of the tracking inefficiency. However, the TPC track

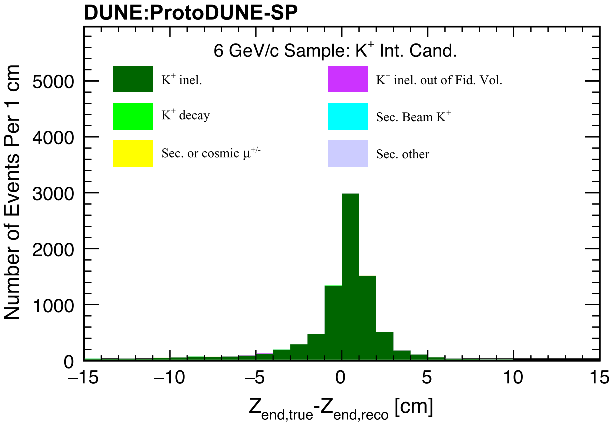

FIG. 14. Difference in the endpoint along the detector length (Z) between the truth-level information and the calibrated reconstructed information for the 6 GeV/c simulation sample. The mean offset measured in the 6 GeV/c simulation sample is 0.539 cm with a standard deviation of 1.231 cm using a Gaussian fit.

TABLE V. Percent deviations from central-value data results by throwing positive one and negative one standard deviation shifts of the uncertainty parameters for the 7 GeV/c sample.

Uncertainty source ($^{+1\sigma}_{-1\sigma}$)	5520–6320 MeV (%)	6320–7120 MeV (%)
Beam modeling	−2.38 −3.44	2.16 −0.10
dE/dx calibration	0.69 −0.61	0.18 1.41
Space charge effect	−0.06 0.85	0.07 2.76
GEANT4 modeling	4.12 −4.23	2.57 −1.05
Electron diverter effect	3.77 −3.46	−1.69 3.46
Vertex identification	5.94 −7.24	14.76 −12.00
Events without a track	0.45 −0.56	1.50 −0.20
Simulation statistics	−1.87 2.04	−2.59 3.05
Data statistics	−0.79 −5.03	3.57 −1.46
All uncertainties	8.78 11.18	15.93 13.34

reconstruction may still have discrepancies in performance between data and simulation not covered by the space charge effect systematic uncertainty. Therefore, an uncertainty of 6% is applied to events without a TPC track, which is a conservative value from the measurements of the efficiency for selecting a beam particle in Ref. [22].

Table IV shows the ±1σ shifts for data from the 6 GeV/c beamline setting. Table V reveals the same shifts for data from the 7 GeV/c beamline setting. The dominant uncertainties are the vertex identification uncertainty and the uncertainties on the GEANT4 model used in the simulation. The former can be improved with in-depth vertexing studies on how the reconstruction delineates vertices and how much energy is required to create a vertex or to stitch the parent and secondary. The latter could be improved with the reduction of the background of secondary kaons reconstructed as the beam particle as the uncertainty alters the frequency of all kaons in simulation, even those in events where the background is selected by the TPC track reconstruction. There is currently no known way to reduce the TPC track selection choosing a secondary kaons, as the dE/dx would be nearly identical to that of beam kaons.

IX. CONCLUSIONS

This paper describes a measurement of the total inelastic cross section of positively charged kaons on argon with the

TABLE IV. Percent deviations from central-value data results by throwing positive one and negative one standard deviation shifts of the uncertainty parameters for the 6 GeV/c sample.

Uncertainty source ($^{+1\sigma}_{-1\sigma}$)	4480–5080 MeV (%)	5080–5340 MeV (%)	5340–5610 MeV (%)	5610–6170 MeV (%)
Beam modeling	−1.79 1.58	2.50 −3.89	−0.74 1.71	4.01 0.51
dE/dx calibration	0.94 1.59	−0.71 −0.76	−0.96 −1.69	1.92 1.66
Space charge effect	1.28 1.92	−1.18 0.76	−2.04 0.28	2.05 4.42
GEANT4 modeling	6.84 −4.60	3.72 −5.60	1.98 −5.16	4.32 −0.64
Electron diverter effect	6.54 −1.24	3.11 −2.68	1.64 −2.73	2.42 3.43
Vertex identification	8.55 −6.25	9.37 −10.57	7.93 −10.18	13.44 −8.28
Events without a track	1.61 1.22	−0.29 −1.40	−1.05 −1.83	2.70 1.27
Simulation statistics	−0.90 0.89	−1.81 2.12	−1.54 1.76	−2.27 2.48
Data statistics	2.65 −2.27	−4.80 −9.77	5.35 −0.06	6.58 −0.56
All uncertainties	13.38 8.82	12.08 16.38	10.35 12.25	16.88 10.56

ProtoDUNE-SP detector using the *thin slice method* [25]. This measurement was done with data taken at the H4-VLE at the CERN Neutrino Platform. A simple event selection achieved a purity of approximately 85-90% between kinetic energies of 4.5 and 7.0 GeV (Table I). The results, at around 380 mbarns, have a precision of approximately 14%, according to Tables II and III. The total uncertainty almost entirely comes from systematic uncertainties addressing the detector model and uncertainties regarding the kaon cross-section model used in GEANT4. The measurements translate to GEANT4 overestimating the cross section by 16% and GENIE overestimating the cross section by 19%. For the 6 GeV/c data sample, the reduced chi-square statistic measured is 11.26/4 bins with GEANT4 and 13.33/4 bins with GENIEhA2018, suggesting tension with both models.

Future studies can utilize the results for tuning kaon reaction scattering models incorporated in various hadron interaction event generators. The upcoming ProtoDUNE Horizontal Drift detector will also exist in the same detector hall with a wire-based readout and can measure similar cross sections with nearly identical methods. It may also run with the beam polarity reversed, allowing for a cross section analysis of negatively charged kaons.

ACKNOWLEDGMENTS

The ProtoDUNE-SP detector was constructed and operated on the CERN Neutrino Platform. We gratefully acknowledge the support of the CERN management and the CERN EP, BE, TE, EN, and IT Departments for NP04/ProtoDUNE-SP. This document was prepared by the DUNE collaboration using the resources of the Fermi National Accelerator Laboratory (Fermilab), a U.S. Department of Energy, Office of Science, HEP User Facility. Fermilab is managed by Fermi Research Alliance, LLC (FRA), acting under Contract No. DE-AC02-07CH11359. This work was supported by CNPq, FAPERJ, FAPEG, and FAPESP, Brazil; CFI, IPP, and NSERC, Canada; CERN; MŠMT, Czech Republic; ERDF, H2020-EU, and MSCA, European Union; CNRS/IN2P3 and CEA, France; INFN, Italy; FCT, Portugal; NRF, South Korea; CAM, Fundación "La Caixa," Junta de Andalucía-FEDER, MICINN, and Xunta de Galicia, Spain; SERI and SNSF, Switzerland; TÜBİTAK, Turkey; The Royal Society and UKRI/STFC, United Kingdom; DOE and NSF, United States of America.

APPENDIX: DISTRIBUTIONS OF THE 7 GeV/c BEAM EVENT SELECTION

This appendix contains the distributions for the 7 GeV/c samples for the event selection in simulation and data. The distribution of tracks without the event selection are shown in Fig. 15. The distribution for all selected kaons and

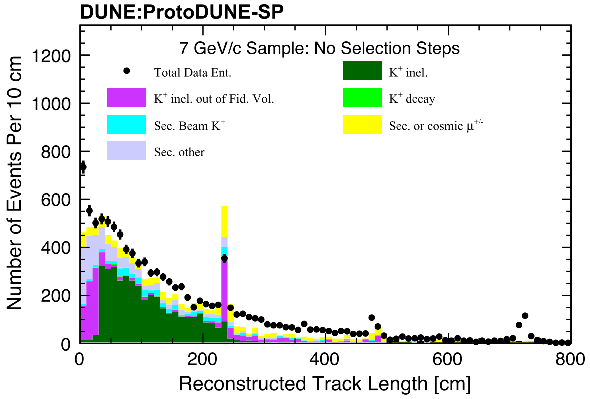

FIG. 15. Reconstructed track length for simulation and data without any selection steps for the 7 GeV/c samples. The statistics are scaled to match the statistics of the data, regardless of if the event had a TPC track. Only statistical uncertainties from the data are shown.

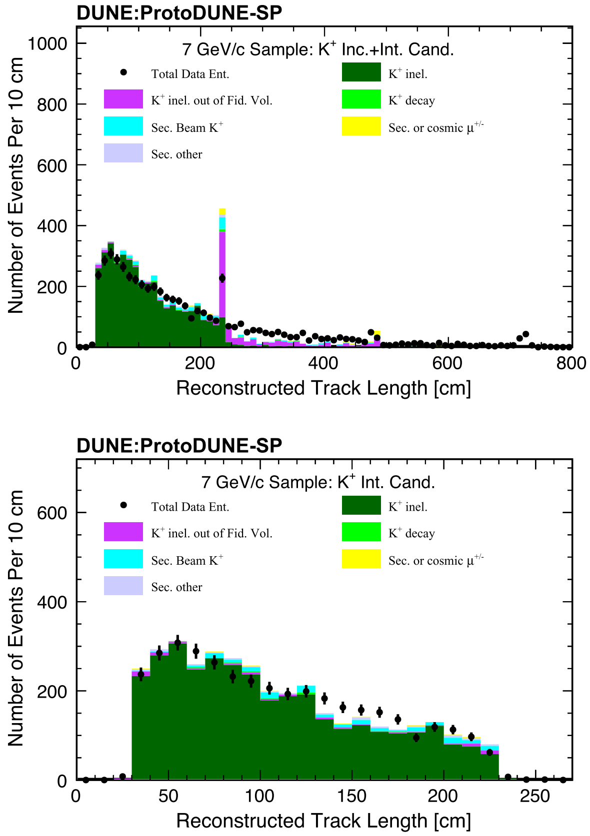

FIG. 16. Reconstructed track length for simulation and data for the 7 GeV/c samples both for all selected kaons (top) and only selected kaons with interacting slices in the fiducial volume (bottom). The statistics are scaled to match the statistics of the data. Only statistical uncertainties from the data are shown.

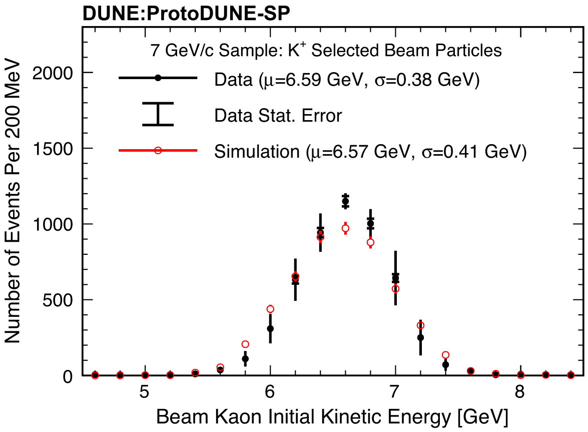

FIG. 17. Initial beam particle kinetic energy as measured by the beamline instrumentation for selected kaon candidate tracks for the 7 GeV/c beamline setting. Both systematic and statistical uncertainties are shown.

selected kaons with interactions in the fiducial volume are shown in Fig. 16. The initial beamline kinetic energy distributions for all selected beam kaons at this beamline setting, as measured by the beamline instrumentation, are shown in Fig. 17.

All distributions show agreements with similar distributions in the 6 GeV/c sample, as seen in Fig. 4. Furthermore, similar purities and slightly lower efficiencies in incident and interacting slice distributions can be observed in Fig. 18.

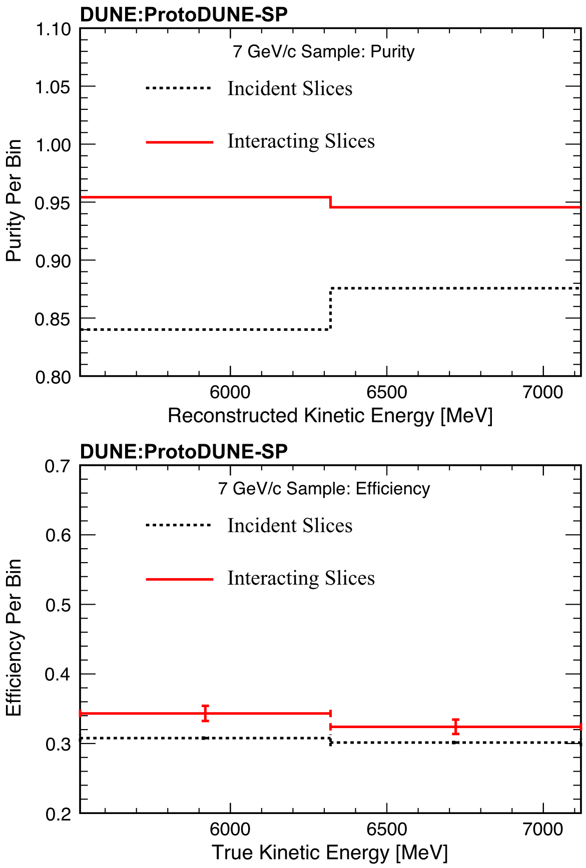

FIG. 18. Purity (top) and efficiency (bottom) of the event selection for each bin for the 7 GeV/c simulation sample.

[1] B. Abi *et al.* (DUNE Collaboration), DUNE technical design report volume I. Introduction to DUNE, J. Instrum. **15**, T08008 (2020).

[2] N. Sakai and T. Yanagida, Proton decay in a class of supersymmetric grand unified models, Nucl. Phys. **B197**, 533 (1982).

[3] S. Weinberg, Supersymmetry at ordinary energies. 1. Masses and conservation laws, Phys. Rev. D **26**, 287 (1982).

[4] S. Dimopoulos, S. Raby, and F. Wilczek, Proton decay in supersymmetric models, Phys. Lett. B **112**, 133 (1982).

[5] S. Dimopoulos and H. Georgi, Softly broken supersymmetry and SU(5), Nucl. Phys. **B193**, 150 (1981).

[6] P. Nath, A. H. Chamseddine, and R. L. Arnowitt, Nucleon decay in supergravity unified theories, Phys. Rev. D **32**, 2348 (1985).

[7] K. Abe *et al.* (Super-Kamiokande Collaboration), Search for proton decay via $p \to \nu K^+$ using 260 kiloton · year data of Super-Kamiokande, Phys. Rev. D **90**, 072005 (2014).

[8] B. Abi *et al.* (DUNE Collaboration), First results on ProtoDUNE-SP liquid argon time projection chamber performance from a beam test at the CERN neutrino platform, J. Instrum. **15**, P12004 (2020).

[9] A. A. Abud *et al.*, Design, construction and operation of the ProtoDUNE-SP liquid argon TPC, J. Instrum. **17**, P01005 (2022).

[10] C. Andreopoulos *et al.*, The GENIE neutrino Monte Carlo generator, Nucl. Instrum. Methods Phys. Res., Sect. A **614**, 87 (2010).

[11] C. Andreopoulos, C. Barry, S. Dytman, H. Gallagher, T. Golan, R. Hatcher, G. Perdue, and J. Yarba, The GENIE neutrino Monte Carlo generator: Physics and user manual, arXiv:1510.05494.

[12] J. Tena-Vidal *et al.* (GENIE Collaboration), Neutrino-nucleon cross-section model tuning in GENIE v3, Phys. Rev. D **104**, 072009 (2021).

[13] J. Tena-Vidal *et al.* (GENIE Collaboration), Hadronization model tuning in GENIE v3, Phys. Rev. D **105**, 012009 (2022).

[14] S. Dytman, Y. Hayato, R. Raboanary, J. T. Sobczyk, J. Tena Vidal, and N. Vololoniaina, Comparison of validation methods of simulations for final state interactions in hadron

production experiments, Phys. Rev. D **104**, 053006 (2021).

[15] S. Agostinelli *et al.*, GEANT4—a simulation toolkit, Nucl. Instrum. Methods Phys. Res., Sect. A **506**, 250 (2003).

[16] J. Allison *et al.*, Geant4 developments and applications, IEEE Trans. Nucl. Sci. **53**, 270 (2006).

[17] J. Allison *et al.*, Recent developments in GEANT4, Nucl. Instrum. Methods Phys. Res., Sect. A **835**, 186 (2016).

[18] J. Calcutt, C. Thorpe, K. Mahn, and L. Fields, Geant4Reweight: A framework for evaluating and propagating hadronic interaction uncertainties in Geant4, J. Instrum. **16**, P08042 (2021).

[19] S. Palestini, Space charge effects in noble liquid calorimeters and time projection chambers, Instruments **5**, 9 (2021).

[20] A. C. Booth, N. Charitonidis, P. Chatzidaki, Y. Karyotakis, E. Nowak, I. Ortega-Ruiz, M. Rosenthal, and P. Sala, Particle production, transport, and identification in the regime of 1–7 GeV/*c*, Phys. Rev. Accel. Beams **22**, 061003 (2019).

[21] J. S. Marshall and M. A. Thomson, The Pandora software development kit for pattern recognition, Eur. Phys. J. C **75**, 439 (2015).

[22] A. Abed Abud *et al.* (DUNE Collaboration), Reconstruction of interactions in the ProtoDUNE-SP detector with Pandora, Eur. Phys. J. C **83**, 618 (2023).

[23] R. Acciarri *et al.* (MicroBooNE Collaboration), The Pandora multi-algorithm approach to automated pattern recognition of cosmic-ray muon and neutrino events in the MicroBooNE detector, Eur. Phys. J. C **78**, 82 (2018).

[24] E. Gramellini, Measurement of the negative pion and positive kaon total hadronic cross sections on argon at the LArIAT experiment, Ph.D. thesis, Yale University, 2018.

[25] E. Gramellini *et al.* (LArIAT Collaboration), Measurement of the π^--Ar total hadronic cross section at the LArIAT experiment, Phys. Rev. D **106**, 052009 (2022).

[26] G. D'Agostini, A multidimensional unfolding method based on Bayes' theorem, Nucl. Instrum. Methods Phys. Res., Sect. A **362**, 487 (1995).

[27] W. H. Richardson, Bayesian-based iterative method of image restoration*, J. Opt. Soc. Am. **62**, 55 (1972).

[28] L. B. Lucy, An iterative technique for the rectification of observed distributions, Astron. J. **79**, 745 (1974).

[29] L. Brenner, R. Balasubramanian, C. Burgard, W. Verkerke, G. Cowan, P. Verschuuren, and V. Croft, Comparison of unfolding methods using RooFitUnfold, Int. J. Mod. Phys. A **35**, 2050145 (2020).

[30] RooUnfold, https://gitlab.cern.ch/RooUnfold/RooUnfold (2023).

[31] J. Tena-Vidal *et al.* (GENIE Collaboration), Hadronization model tuning in GENIE v3, Phys. Rev. D **105**, 012009 (2022).

[32] R. A. Arndt, W. J. Briscoe, I. I. Strakovsky, and R. L. Workman, Extended partial-wave analysis of πN scattering data, Phys. Rev. C **74**, 045205 (2006).

[33] R. L. Workman, V. D. Burkert, V. Crede, E. Klempt, U. Thoma, L. Tiator *et al.* (Particle Data Group), Review of particle physics, Prog. Theor. Exp. Phys. **2022**, 083C01 (2022).

[34] B. P. Roe, Statistical errors in Monte Carlo estimates of systematic errors, Nucl. Instrum. Methods Phys. Res., Sect. A **570**, 159 (2007).

[35] J. Calcutt, Measurement of π^+—argon absorption and charge exchange interactions using ProtoDUNE-SP, Ph.D. thesis, Michigan State U., 2021.

[36] R. Diurba, Evaluating the ProtoDUNE-SP detector performance to measure a 6 GeV/c positive kaon inelastic cross section on argon, Ph.D. thesis, Minnesota U., 2021.

[37] C. Adams *et al.* (MicroBooNE Collaboration), Calibration of the charge and energy loss per unit length of the MicroBooNE liquid argon time projection chamber using muons and protons, J. Instrum. **15**, P03022 (2020).

A. Abed Abud,[35] B. Abi,[156] R. Acciarri,[66] M. A. Acero,[12] M. R. Adames,[193] G. Adamov,[72] M. Adamowski,[66] D. Adams,[20] M. Adinolfi,[19] C. Adriano,[30] A. Aduszkiewicz,[81] J. Aguilar,[126] F. Akbar,[175] K. Allison,[43] S. Alonso Monsalve,[35] M. Alrashed,[119] A. Alton,[13] R. Alvarez,[39] T. Alves,[88] H. Amar,[84] P. Amedo,[85,84] J. Anderson,[8] C. Andreopoulos,[128] M. Andreotti,[94,67] M. P. Andrews,[66] F. Andrianala,[5] S. Andringa,[127] N. Anfimov,[†] A. Ankowski,[184] D. Antic,[19] M. Antoniassi,[193] M. Antonova,[84] A. Antoshkin,[†] A. Aranda-Fernandez,[42] L. Arellano,[135] E. Arrieta Diaz,[180] M. A. Arroyave,[66] J. Asaadi,[197] A. Ashkenazi,[194] D. Asner,[20] L. Asquith,[191] E. Atkin,[88] D. Auguste,[160] A. Aurisano,[40] V. Aushev,[124] D. Autiero,[110] M. B. Azam,[87] F. Azfar,[156] A. Back,[91] H. Back,[157] J. J. Back,[209] I. Bagaturia,[72] L. Bagby,[66] N. Balashov,[†] S. Balasubramanian,[66] P. Baldi,[24] W. Baldini,[94] J. Baldonedo,[206] B. Baller,[66] B. Bambah,[82] R. Banerjee,[216] F. Barao,[127,112] D. Barbu,[21] G. Barenboim,[84] P. Barham Alzás,[35] G. J. Barker,[209] W. Barkhouse,[148] G. Barr,[156] J. Barranco Monarca,[77] A. Barros,[193] N. Barros,[127,61] D. Barrow,[156] J. L. Barrow,[143] A. Basharina-Freshville,[203] A. Bashyal,[8] V. Basque,[66] C. Batchelor,[57] L. Bathe-Peters,[156] J. B. R. Battat,[210] F. Battisti,[156] F. Bay,[4] M. C. Q. Bazetto,[30] J. L. L. Bazo Alba,[169] J. F. Beacom,[154] E. Bechetoille,[110] B. Behera,[186] E. Belchior,[130] G. Bell,[52] L. Bellantoni,[66] G. Bellettini,[103,167] V. Bellini,[93,31] O. Beltramello,[35] N. Benekos,[35] C. Benitez Montiel,[84,10] D. Benjamin,[20] F. Bento Neves,[127] J. Berger,[44] S. Berkman,[139] J. Bernal,[10] P. Bernardini,[97,179] A. Bersani,[96] S. Bertolucci,[92,17] M. Betancourt,[66] A. Betancur Rodríguez,[58] A. Bevan,[172] Y. Bezawada,[23] A. T. Bezerra,[62] T. J. Bezerra,[191] A. Bhat,[37] V. Bhatnagar,[159]

J. Bhatt,[203] M. Bhattacharjee,[89] M. Bhattacharya,[66] S. Bhuller,[19] B. Bhuyan,[89] S. Biagi,[105] J. Bian,[24] K. Biery,[66]
B. Bilki,[15,108] M. Bishai,[20] A. Bitadze,[135] A. Blake,[125] F. D. Blaszczyk,[66] G. C. Blazey,[149] E. Blucher,[37]
A. Bodek,[175] J. Bogenschuetz,[197] J. Boissevain,[129] S. Bolognesi,[34] T. Bolton,[119] L. Bomben,[98,107] M. Bonesini,[98,140]
C. Bonilla-Diaz,[32] F. Bonini,[20] A. Booth,[172] F. Boran,[91] S. Bordoni,[35] R. Borges Merlo,[30] A. Borkum,[191]
N. Bostan,[108] R. Bouet,[131] J. Boza,[44] J. Bracinik,[16] B. Brahma,[90] D. Brailsford,[125] F. Bramati,[98] A. Branca,[98]
A. Brandt,[197] J. Bremer,[35] C. Brew,[178] S. J. Brice,[66] V. Brio,[93] C. Brizzolari,[98,140] C. Bromberg,[139] J. Brooke,[19]
A. Bross,[66] G. Brunetti,[98,140] M. Brunetti,[209] N. Buchanan,[44] H. Budd,[175] J. Buergi,[14] A. Bundock,[19]
D. Burgardt,[211] S. Butchart,[191] V. G. Caceres,[23] I. Cagnoli,[92,17] T. Cai,[216] R. Calabrese,[100] R. Calabrese,[94,67]
J. Calcutt,[155] L. Calivers,[14] E. Calvo,[39] A. Caminata,[96] A. F. Camino,[168] W. Campanelli,[127] A. Campani,[96,71]
A. Campos Benitez,[207] N. Canci,[100] J. Capó,[84] I. Caracas,[134] D. Caratelli,[27] D. Carber,[44] J. M. Carceller,[35] G. Carini,[20]
B. Carlus,[110] M. F. Carneiro,[20] P. Carniti,[98] I. Caro Terrazas,[44] H. Carranza,[197] N. Carrara,[23] L. Carroll,[119] T. Carroll,[213]
A. Carter,[176] E. Casarejos,[206] D. Casazza,[94] J. F. Castaño Forero,[7] F. A. Castaño,[6] A. Castillo,[182] C. Castromonte,[106]
E. Catano-Mur,[212] C. Cattadori,[98] F. Cavalier,[160] F. Cavanna,[66] S. Centro,[158] G. Cerati,[66] C. Cerna,[131]
A. Cervelli,[92] A. Cervera Villanueva,[84] K. Chakraborty,[166] S. Chakraborty,[86] M. Chalifour,[35] A. Chappell,[209]
N. Charitonidis,[35] A. Chatterjee,[166] H. Chen,[20] M. Chen,[24] W. C. Chen,[199] Y. Chen,[184] Z. Chen-Wishart,[176]
D. Cherdack,[81] C. Chi,[45] F. Chiapponi,[92] R. Chirco,[87] N. Chitirasreemadam,[103,167] K. Cho,[122] S. Choate,[108]
D. Chokheli,[72] P. S. Chong,[164] B. Chowdhury,[8] D. Christian,[66] A. Chukanov,[†] M. Chung,[202] E. Church,[157]
M. F. Cicala,[203] M. Cicerchia,[158] V. Cicero,[92,17] R. Ciolini,[103] P. Clarke,[57] G. Cline,[126] T. E. Coan,[188] A. G. Cocco,[100]
J. A. B. Coelho,[161] A. Cohen,[161] J. Collazo,[206] J. Collot,[76] E. Conley,[55] J. M. Conrad,[136] M. Convery,[184] S. Copello,[96]
P. Cova,[99,162] C. Cox,[176] L. Cremaldi,[144] L. Cremonesi,[172] J. I. Crespo-Anadón,[39] M. Crisler,[66] E. Cristaldo,[98,10]
J. Crnkovic,[66] G. Crone,[203] R. Cross,[209] A. Cudd,[43] C. Cuesta,[39] Y. Cui,[26] F. Curciarello,[95] D. Cussans,[19]
J. Dai,[76] O. Dalager,[66] R. Dallavalle,[161] W. Dallaway,[199] R. D’Amico,[94,67] H. da Motta,[33] Z. A. Dar,[212] R. Darby,[191]
L. Da Silva Peres,[65] Q. David,[110] G. S. Davies,[144] S. Davini,[96] J. Dawson,[161] R. De Aguiar,[30] P. De Almeida,[30]
P. Debbins,[108] I. De Bonis,[51] M. P. Decowski,[146,3] A. de Gouvêa,[150] P. C. De Holanda,[30] I. L. De Icaza Astiz,[191]
P. De Jong,[146,3] P. Del Amo Sanchez,[51] A. De la Torre,[39] G. De Lauretis,[110] A. Delbart,[34] D. Delepine,[77]
M. Delgado,[98,140] A. Dell’Acqua,[35] G. Delle Monache,[95] N. Delmonte,[99,162] P. De Lurgio,[8] R. Demario,[139]
G. De Matteis,[97] J. R. T. de Mello Neto,[65] D. M. DeMuth,[205] S. Dennis,[29] C. Densham,[178] P. Denton,[20]
G. W. Deptuch,[20] A. De Roeck,[35] V. De Romeri,[84] J. P. Detje,[29] J. Devine,[35] R. Dharmapalan,[79] M. Dias,[201]
A. Diaz,[28] J. S. Díaz,[91] F. Díaz,[169] F. Di Capua,[100,145] A. Di Domenico,[181,104] S. Di Domizio,[96,71] S. Di Falco,[103]
L. Di Giulio,[35] P. Ding,[66] L. Di Noto,[96,71] E. Diociaiuti,[95] C. Distefano,[105] R. Diurba,[14] M. Diwan,[20] Z. Djurcic,[8]
D. Doering,[184] S. Dolan,[35] F. Dolek,[207] M. J. Dolinski,[54] D. Domenici,[95] L. Domine,[184] S. Donati,[103,167]
Y. Donon,[35] S. Doran,[109] D. Douglas,[184] T. A. Doyle,[189] A. Dragone,[184] F. Drielsma,[184] L. Duarte,[201]
D. Duchesneau,[51] K. Duffy,[156] K. Dugas,[24] P. Dunne,[88] B. Dutta,[195] H. Duyang,[185] D. A. Dwyer,[126]
A. S. Dyshkant,[149] S. Dytman,[168] M. Eads,[149] A. Earle,[191] S. Edayath,[109] D. Edmunds,[139] J. Eisch,[66] P. Englezos,[177]
A. Ereditato,[37] T. Erjavec,[23] C. O. Escobar,[66] J. J. Evans,[135] E. Ewart,[91] A. C. Ezeribe,[183] K. Fahey,[66] L. Fajt,[35]
A. Falcone,[98,140] M. Fani’,[143,129] C. Farnese,[101] S. Farrell,[174] Y. Farzan,[111] D. Fedoseev,[†] J. Felix,[77] Y. Feng,[109]
E. Fernandez-Martinez,[133] G. Ferry,[160] E. Fialova,[50] L. Fields,[151] P. Filip,[49] A. Filkins,[192] F. Filthaut,[146,173]
R. Fine,[129] G. Fiorillo,[100,145] M. Fiorini,[94,67] S. Fogarty,[44] W. Foreman,[87] J. Fowler,[55] J. Franc,[50] K. Francis,[149]
D. Franco,[37] J. Franklin,[56] J. Freeman,[66] J. Fried,[20] A. Friedland,[184] S. Fuess,[66] I. K. Furic,[68] K. Furman,[172]
A. P. Furmanski,[143] R. Gaba,[159] A. Gabrielli,[92,17] A. M. Gago,[169] F. Galizzi,[98] H. Gallagher,[200] N. Gallice,[20]
V. Galymov,[110] E. Gamberini,[35] T. Gamble,[183] F. Ganacim,[193] R. Gandhi,[78] S. Ganguly,[66] F. Gao,[27] S. Gao,[20]
D. Garcia-Gamez,[73] M. Á. García-Peris,[84] F. Gardim,[62] S. Gardiner,[66] D. Gastler,[18] A. Gauch,[14] J. Gauvreau,[153]
P. Gauzzi,[181,104] S. Gazzana,[95] G. Ge,[45] N. Geffroy,[51] B. Gelli,[30] S. Gent,[187] L. Gerlach,[20]
Z. Ghorbani-Moghaddam,[96] T. Giammaria,[94,67] D. Gibin,[158,101] I. Gil-Botella,[39] S. Gilligan,[155] A. Gioiosa,[103]
S. Giovannella,[95] C. Girerd,[110] A. K. Giri,[90] C. Giugliano,[94] V. Giusti,[103] D. Gnani,[126] O. Gogota,[124]
S. Gollapinni,[129] K. Gollwitzer,[66] R. A. Gomes,[63] L. V. Gomez Bermeo,[182] L. S. Gomez Fajardo,[182] F. Gonnella,[16]
D. Gonzalez-Diaz,[85] M. Gonzalez-Lopez,[133] M. C. Goodman,[8] S. Goswami,[166] C. Gotti,[98] J. Goudeau,[130]
E. Goudzovski,[16] C. Grace,[126] E. Gramellini,[135] R. Gran,[142] E. Granados,[77] P. Granger,[161] C. Grant,[18]
D. R. Gratieri,[70,30] G. Grauso,[100] P. Green,[156] S. Greenberg,[126,22] J. Greer,[19] W. C. Griffith,[191] F. T. Groetschla,[35]

K. Grzelak,[208] L. Gu,[125] W. Gu,[20] V. Guarino,[8] M. Guarise,[94,67] R. Guenette,[135] M. Guerzoni,[92] D. Guffanti,[98,140]
A. Guglielmi,[101] B. Guo,[185] F. Y. Guo,[189] A. Gupta,[184] V. Gupta,[146,3] G. Gurung,[197] D. Gutierrez,[170] P. Guzowski,[135]
M. M. Guzzo,[30] S. Gwon,[38] A. Habig,[142] H. Hadavand,[197] L. Haegel,[110] R. Haenni,[14] L. Hagaman,[214] A. Hahn,[66]
J. Haiston,[186] J. Hakenmüller,[55] T. Hamernik,[66] P. Hamilton,[88] J. Hancock,[16] F. Happacher,[95] D. A. Harris,[216,66]
A. Hart,[172] J. Hartnell,[191] T. Hartnett,[178] J. Harton,[44] T. Hasegawa,[121] C. M. Hasnip,[35] R. Hatcher,[66]
K. Hayrapetyan,[172] J. Hays,[172] E. Hazen,[18] M. He,[81] A. Heavey,[66] K. M. Heeger,[214] J. Heise,[190] P. Hellmuth,[131]
S. Henry,[175] K. Herner,[66] V. Hewes,[40] A. Higuera Pichardo,[174] C. Hilgenberg,[143] S. J. Hillier,[16] A. Himmel,[66]
E. Hinkle,[37] L. R. Hirsch,[193] J. Ho,[53] J. Hoff,[66] A. Holin,[178] T. Holvey,[156] E. Hoppe,[157] S. Horiuchi,[207]
G. A. Horton-Smith,[119] T. Houdy,[160] B. Howard,[216] R. Howell,[175] I. Hristova,[178] M. S. Hronek,[66] J. Huang,[23]
R. G. Huang,[126] Z. Hulcher,[184] M. Ibrahim,[59] G. Iles,[88] N. Ilic,[199] A. M. Iliescu,[95] R. Illingworth,[66] G. Ingratta,[92,17]
A. Ioannisian,[215] B. Irwin,[143] L. Isenhower,[1] M. Ismerio Oliveira,[65] R. Itay,[184] C. M. Jackson,[157] V. Jain,[2]
E. James,[66] W. Jang,[197] B. Jargowsky,[24] D. Jena,[66] I. Jentz,[213] X. Ji,[20] C. Jiang,[115] J. Jiang,[189] L. Jiang,[207] A. Jipa,[21]
J. H. Jo,[20] F. R. Joaquim,[127,112] W. Johnson,[186] C. Jollet,[131] B. Jones,[197] R. Jones,[183] N. Jovancevic,[152] M. Judah,[168]
C. K. Jung,[189] T. Junk,[66] Y. Jwa,[184,45] M. Kabirnezhad,[88] A. C. Kaboth,[176,178] I. Kadenko,[124] I. Kakorin,[†]
A. Kalitkina,[†] D. Kalra,[45] M. Kandemir,[60] D. M. Kaplan,[87] G. Karagiorgi,[45] G. Karaman,[108] A. Karcher,[126]
Y. Karyotakis,[51] S. Kasai,[123] S. P. Kasetti,[130] L. Kashur,[44] I. Katsioulas,[16] A. Kauther,[149] N. Kazaryan,[215] L. Ke,[20]
E. Kearns,[18] P. T. Keener,[164] K. J. Kelly,[195] E. Kemp,[30] O. Kemularia,[72] Y. Kermaidic,[160] W. Ketchum,[66]
S. H. Kettell,[20] M. Khabibullin,[†] N. Khan,[88] A. Khvedelidze,[72] D. Kim,[195] J. Kim,[175] M. J. Kim,[66] B. King,[66]
B. Kirby,[45] M. Kirby,[20] A. Kish,[66] J. Klein,[164] J. Kleykamp,[144] A. Klustova,[88] T. Kobilarcik,[66] L. Koch,[134]
K. Koehler,[213] L. W. Koerner,[81] D. H. Koh,[184] L. Kolupaeva,[†] D. Korablev,[†] M. Kordosky,[212] T. Kosc,[76]
U. Kose,[35] V. A. Kostelecký,[91] K. Kothekar,[19] I. Kotler,[54] M. Kovalcuk,[49] V. Kozhukalov,[†] W. Krah,[146] R. Kralik,[191]
M. Kramer,[126] L. Kreczko,[19] F. Krennrich,[109] I. Kreslo,[14] T. Kroupova,[164] S. Kubota,[135] M. Kubu,[35] Y. Kudenko,[†]
V. A. Kudryavtsev,[183] G. Kufatty,[69] S. Kuhlmann,[8] S. Kulagin,[†] J. Kumar,[79] P. Kumar,[183] S. Kumaran,[24]
J. Kunzmann,[14] R. Kuravi,[126] N. Kurita,[184] C. Kuruppu,[185] V. Kus,[50] T. Kutter,[130] J. Kvasnicka,[49] T. Labree,[149]
T. Lackey,[66] I. Lalău,[21] A. Lambert,[126] B. J. Land,[164] C. E. Lane,[54] N. Lane,[135] K. Lang,[198] T. Langford,[214]
M. Langstaff,[135] F. Lanni,[35] O. Lantwin,[51] J. Larkin,[20] P. Lasorak,[88] D. Last,[164] A. Laudrain,[134] A. Laundrie,[213]
G. Laurenti,[92] E. Lavaut,[160] P. Laycock,[20] I. Lazanu,[21] R. LaZur,[44] M. Lazzaroni,[99,141] T. Le,[200] S. Leardini,[85]
J. Learned,[79] T. LeCompte,[184] V. Legin,[124] G. Lehmann Miotto,[35] R. Lehnert,[91] M. A. Leigui de Oliveira,[64]
M. Leitner,[126] D. Leon Silverio,[186] L. M. Lepin,[69] J.-Y Li,[57] S. W. Li,[24] Y. Li,[20] H. Liao,[119] C. S. Lin,[126]
D. Lindebaum,[19] S. Linden,[20] R. A. Lineros,[32] A. Lister,[213] B. R. Littlejohn,[87] H. Liu,[20] J. Liu,[24] Y. Liu,[37]
S. Lockwitz,[66] M. Lokajicek,[49] I. Lomidze,[72] K. Long,[88] T. V. Lopes,[62] J. H. Lopez Botero,[6] I. López de Rego,[39]
N. López-March,[84] T. Lord,[209] J. M. LoSecco,[151] W. C. Louis,[129] A. Lozano Sanchez,[54] X.-G. Lu,[209] K. B. Luk,[80,126,22]
B. Lunday,[164] X. Luo,[27] E. Luppi,[94,67] D. MacFarlane,[184] A. A. Machado,[30] P. Machado,[66] C. T. Macias,[91]
J. R. Macier,[66] M. MacMahon,[203] A. Maddalena,[75] A. Madera,[35] P. Madigan,[22,126] S. Magill,[8] C. Magueur,[160]
K. Mahn,[139] A. Maio,[127,61] A. Major,[55] K. Majumdar,[128] S. Mameli,[103] M. Man,[199] R. C. Mandujano,[24] J. Maneira,[127,61]
S. Manly,[175] A. Mann,[200] K. Manolopoulos,[178] M. Manrique Plata,[91] S. Manthey Corchado,[39] V. N. Manyam,[20]
M. Marchan,[66] A. Marchionni,[66] W. Marciano,[20] D. Marfatia,[79] C. Mariani,[207] J. Maricic,[79] F. Marinho,[113]
A. D. Marino,[43] T. Markiewicz,[184] F. Das Chagas Marques,[30] C. Marquet,[131] M. Marshak,[143] C. M. Marshall,[175]
J. Marshall,[209] L. Martina,[97] J. Martín-Albo,[84] N. Martinez,[119] D. A. Martinez Caicedo,[186] F. Martínez López,[172]
P. Martínez Miravé,[84] S. Martynenko,[20] V. Mascagna,[98] C. Massari,[98] A. Mastbaum,[177] F. Matichard,[126] S. Matsuno,[79]
G. Matteucci,[100,145] J. Matthews,[130] C. Mauger,[164] N. Mauri,[92,17] K. Mavrokoridis,[128] I. Mawby,[125] R. Mazza,[98]
T. McAskill,[210] N. McConkey,[172,203] K. S. McFarland,[175] C. McGrew,[189] A. McNab,[135] L. Meazza,[98]
V. C. N. Meddage,[68] A. Mefodiev,[†] B. Mehta,[159] P. Mehta,[116] P. Melas,[11] O. Mena,[84] H. Mendez,[170] P. Mendez,[35]
D. P. Méndez,[20] A. Menegolli,[102,163] G. Meng,[101] A. C. E. A. Mercuri,[193] A. Meregaglia,[131] M. D. Messier,[91]
S. Metallo,[143] W. Metcalf,[130] M. Mewes,[91] H. Meyer,[211] T. Miao,[66] J. Micallef,[200,136] A. Miccoli,[97] G. Michna,[187]
R. Milincic,[79] F. Miller,[213] G. Miller,[135] W. Miller,[143] O. Mineev,[†] A. Minotti,[98,140] L. Miralles Verge,[35]
O. G. Miranda,[41] C. Mironov,[161] S. Miryala,[20] S. Miscetti,[95] C. S. Mishra,[66] P. Mishra,[82] S. R. Mishra,[185]
A. Mislivec,[143] M. Mitchell,[130] D. Mladenov,[35] I. Mocioiu,[165] A. Mogan,[66] N. Moggi,[92,17] R. Mohanta,[82]
T. A. Mohayai,[91] N. Mokhov,[66] J. Molina,[10] L. Molina Bueno,[84] E. Montagna,[92,17] A. Montanari,[92]

C. Montanari,[102,66,163] D. Montanari,[66] D. Montanino,[97,179] L. M. Montaño Zetina,[41] M. Mooney,[44] A. F. Moor,[183]
Z. Moore,[192] D. Moreno,[7] O. Moreno-Palacios,[212] L. Morescalchi,[103] D. Moretti,[98] R. Moretti,[98] C. Morris,[81]
C. Mossey,[66] C. A. Moura,[64] G. Mouster,[125] W. Mu,[66] L. Mualem,[28] J. Mueller,[44] M. Muether,[211]
F. Muheim,[57] A. Muir,[52] M. Mulhearn,[23] D. Munford,[81] L. J. Munteanu,[35] H. Muramatsu,[143] J. Muraz,[76]
M. Murphy,[207] T. Murphy,[192] J. Muse,[143] A. Mytilinaki,[178] J. Nachtman,[108] Y. Nagai,[59] S. Nagu,[132]
R. Nandakumar,[178] D. Naples,[168] S. Narita,[114] A. Navrer-Agasson,[88,135] N. Nayak,[20] M. Nebot-Guinot,[57]
A. Nehm,[134] J. K. Nelson,[212] O. Neogi,[108] J. Nesbit,[213] M. Nessi,[66,35] D. Newbold,[178] M. Newcomer,[164]
R. Nichol,[203] F. Nicolas-Arnaldos,[73] A. Nikolica,[164] J. Nikolov,[152] E. Niner,[66] K. Nishimura,[79] A. Norman,[66]
A. Norrick,[66] P. Novella,[84] A. Nowak,[125] J. A. Nowak,[125] M. Oberling,[8] J. P. Ochoa-Ricoux,[24] S. Oh,[55] S. B. Oh,[66]
A. Olivier,[151] A. Olshevskiy,[†] T. Olson,[81] Y. Onel,[108] Y. Onishchuk,[124] A. Oranday,[91] M. Osbiston,[209]
J. A. Osorio Vélez,[6] L. O'Sullivan,[134] L. Otiniano Ormachea,[46,106] J. Ott,[24] L. Pagani,[23] G. Palacio,[58] O. Palamara,[66]
S. Palestini,[35] J. M. Paley,[66] M. Pallavicini,[96,71] C. Palomares,[39] S. Pan,[166] P. Panda,[82] W. Panduro Vazquez,[176]
E. Pantic,[23] V. Paolone,[168] R. Papaleo,[105] A. Papanestis,[178] D. Papoulias,[11] S. Paramesvaran,[19] A. Paris,[170]
S. Parke,[66] E. Parozzi,[98,140] S. Parsa,[14] Z. Parsa,[20] S. Parveen,[116] M. Parvu,[21] D. Pasciuto,[103] S. Pascoli,[92,17]
L. Pasqualini,[92,17] J. Pasternak,[88] C. Patrick,[57,203] L. Patrizii,[92] R. B. Patterson,[28] T. Patzak,[161] A. Paudel,[66]
L. Paulucci,[64] Z. Pavlovic,[66] G. Pawloski,[143] D. Payne,[128] V. Pec,[49] E. Pedreschi,[103] S. J. M. Peeters,[191]
W. Pellico,[66] A. Pena Perez,[184] E. Pennacchio,[110] A. Penzo,[108] O. L. G. Peres,[30] Y. F. Perez Gonzalez,[56]
L. Pérez-Molina,[39] C. Pernas,[212] J. Perry,[57] D. Pershey,[69] G. Pessina,[98] G. Petrillo,[184] C. Petta,[93,31] R. Petti,[185]
M. Pfaff,[88] V. Pia,[92,17] L. Pickering,[178,176] F. Pietropaolo,[35,101] V. L. Pimentel,[47,30] G. Pinaroli,[20] S. Pincha,[89]
J. Pinchault,[51] K. Pitts,[207] K. Plows,[156] C. Pollack,[170] T. Pollman,[146,3] F. Pompa,[84] X. Pons,[35] N. Poonthottathil,[86,109]
V. Popov,[194] F. Poppi,[92,17] J. Porter,[191] L. G. Porto Paixão,[30] M. Potekhin,[20] R. Potenza,[93,31] J. Pozimski,[88] M. Pozzato,[92,17]
T. Prakash,[126] C. Pratt,[23] M. Prest,[98] F. Psihas,[66] D. Pugnere,[110] X. Qian,[20] J. Queen,[55] J. L. Raaf,[66] V. Radeka,[20]
J. Rademacker,[19] B. Radics,[216] F. Raffaelli,[103] A. Rafique,[8] E. Raguzin,[20] M. Rai,[209] S. Rajagopalan,[20]
M. Rajaoalisoa,[40] I. Rakhno,[66] L. Rakotondravohitra,[5] L. Ralte,[90] M. A. Ramirez Delgado,[164] B. Ramson,[66]
A. Rappoldi,[102,163] G. Raselli,[102,163] P. Ratoff,[125] R. Ray,[66] H. Razafinime,[40] E. M. Rea,[143] J. S. Real,[76]
B. Rebel,[213,66] R. Rechenmacher,[66] J. Reichenbacher,[186] S. D. Reitzner,[66] H. Rejeb Sfar,[35] E. Renner,[129]
A. Renshaw,[81] S. Rescia,[20] F. Resnati,[35] Diego Restrepo,[6] C. Reynolds,[172] M. Ribas,[193] S. Riboldi,[99] C. Riccio,[189]
G. Riccobene,[105] J. S. Ricol,[76] M. Rigan,[191] E. V. Rincón,[58] A. Ritchie-Yates,[176] S. Ritter,[134] D. Rivera,[129] R. Rivera,[66]
A. Robert,[76] J. L. Rocabado Rocha,[84] L. Rochester,[184] M. Roda,[128] P. Rodrigues,[156] M. J. Rodriguez Alonso,[35]
J. Rodriguez Rondon,[186] S. Rosauro-Alcaraz,[160] P. Rosier,[160] D. Ross,[139] M. Rossella,[102,163] M. Rossi,[35]
M. Ross-Lonergan,[129] N. Roy,[216] P. Roy,[211] C. Rubbia,[74] A. Ruggeri,[92] G. Ruiz Ferreira,[135] B. Russell,[136]
D. Ruterbories,[175] A. Rybnikov,[†] S. Sacerdoti,[161] S. Saha,[168] S. K. Sahoo,[90] N. Sahu,[90] P. Sala,[66] N. Samios,[20]
O. Samoylov,[†] M. C. Sanchez,[69] A. Sánchez Bravo,[84] A. Sánchez-Castillo,[73] P. Sánchez-Lucas,[73] V. Sandberg,[129]
D. A. Sanders,[144] S. Sanfilippo,[105] D. Sankey,[178] D. Santoro,[99,162] N. Saoulidou,[11] P. Sapienza,[105] C. Sarasty,[40]
I. Sarcevic,[9] I. Sarra,[95] G. Savage,[66] V. Savinov,[168] G. Scanavini,[214] A. Scaramelli,[102] A. Scarff,[183] T. Schefke,[130]
H. Schellman,[155,66] S. Schifano,[94,67] P. Schlabach,[66] D. Schmitz,[37] A. W. Schneider,[136] K. Scholberg,[55]
A. Schukraft,[66] B. Schuld,[43] A. Segade,[206] E. Segreto,[30] A. Selyunin,[†] D. Senadheera,[168] C. R. Senise Jr.,[201]
J. Sensenig,[164] M. H. Shaevitz,[45] P. Shanahan,[66] P. Sharma,[159] R. Kumar,[171] S. Sharma Poudel,[186] K. Shaw,[191]
T. Shaw,[66] K. Shchablo,[110] J. Shen,[164] C. Shepherd-Themistocleous,[178] A. Sheshukov,[†] J. Shi,[29] W. Shi,[189]
S. Shin,[117] S. Shivakoti,[211] I. Shoemaker,[207] D. Shooltz,[139] R. Shrock,[189] B. Siddi,[94] M. Siden,[44] J. Silber,[126]
L. Simard,[160] J. Sinclair,[184] G. Sinev,[186] Jaydip Singh,[23] J. Singh,[132] L. Singh,[48] P. Singh,[172] V. Singh,[48]
S. Singh Chauhan,[159] R. Sipos,[35] C. Sironneau,[161] G. Sirri,[92] K. Siyeon,[38] K. Skarpaas,[184] J. Smedley,[175] E. Smith,[91]
J. Smith,[189] P. Smith,[91] J. Smolik,[50,49] M. Smy,[24] M. Snape,[209] E. L. Snider,[66] P. Snopok,[87] D. Snowden-Ifft,[153]
M. Soares Nunes,[66] H. Sobel,[24] M. Soderberg,[192] S. Sokolov,[†] C. J. Solano Salinas,[204,106] S. Söldner-Rembold,[88,135]
N. Solomey,[211] V. Solovov,[127] W. E. Sondheim,[129] M. Sorel,[84] A. Sotnikov,[†] J. Soto-Oton,[84] A. Sousa,[40]
K. Soustruznik,[36] F. Spinella,[103] J. Spitz,[138] N. J. C. Spooner,[183] K. Spurgeon,[192] D. Stalder,[10] M. Stancari,[66]
L. Stanco,[158,101] J. Steenis,[23] R. Stein,[19] H. M. Steiner,[126] A. F. Steklain Lisbôa,[193] A. Stepanova,[†] J. Stewart,[20]
B. Stillwell,[37] J. Stock,[186] F. Stocker,[35] T. Stokes,[130] M. Strait,[143] T. Strauss,[66] L. Strigari,[195] A. Stuart,[42]
J. G. Suarez,[58] J. Subash,[16] A. Surdo,[97] L. Suter,[66] C. M. Sutera,[93,31] K. Sutton,[28] Y. Suvorov,[100,145] R. Svoboda,[23]

S. K. Swain,[147] B. Szczerbinska,[196] A. M. Szelc,[57] A. Sztuc,[203] A. Taffara,[103] N. Talukdar,[185] J. Tamara,[7] H. A. Tanaka,[184] S. Tang,[20] N. Taniuchi,[29] A. M. Tapia Casanova,[137] B. Tapia Oregui,[198] A. Tapper,[88] S. Tariq,[66] E. Tarpara,[20] E. Tatar,[83] R. Tayloe,[91] D. Tedeschi,[185] A. M. Teklu,[189] J. Tena Vidal,[194] P. Tennessen,[126,4] M. Tenti,[92] K. Terao,[184] F. Terranova,[98,140] G. Testera,[96] T. Thakore,[40] A. Thea,[178] S. Thomas,[192] A. Thompson,[195] C. Thorn,[20] S. C. Timm,[66] E. Tiras,[60,108] V. Tishchenko,[20] N. Todorović,[152] L. Tomassetti,[94,67] A. Tonazzo,[161] D. Torbunov,[20] M. Torti,[98,140] M. Tortola,[84] F. Tortorici,[93,31] N. Tosi,[92] D. Totani,[27] M. Toups,[66] C. Touramanis,[128] D. Tran,[81] R. Travaglini,[92] J. Trevor,[28] E. Triller,[139] S. Trilov,[19] J. Truchon,[213] D. Truncali,[181,104] W. H. Trzaska,[118] Y. Tsai,[24] Y.-T. Tsai,[184] Z. Tsamalaidze,[72] K. V. Tsang,[184] N. Tsverava,[72] S. Z. Tu,[115] S. Tufanli,[35] C. Tunnell,[174] S. Turnberg,[87] J. Turner,[56] M. Tuzi,[84] J. Tyler,[119] E. Tyley,[183] M. Tzanov,[130] M. A. Uchida,[29] J. Ureña González,[84] J. Urheim,[91] T. Usher,[184] H. Utaegbulam,[175] S. Uzunyan,[149] M. R. Vagins,[120,24] P. Vahle,[212] S. Valder,[191] G. A. Valdiviesso,[62] E. Valencia,[77] R. Valentim,[201] Z. Vallari,[28] E. Vallazza,[98] J. W. F. Valle,[84] R. Van Berg,[164] R. G. Van de Water,[129] D. V. Forero,[137] A. Vannozzi,[95] M. Van Nuland-Troost,[146] F. Varanini,[101] D. Vargas Oliva,[199] S. Vasina,[†] N. Vaughan,[155] K. Vaziri,[66] A. Vázquez-Ramos,[73] J. Vega,[46] S. Ventura,[101] A. Verdugo,[39] S. Vergani,[203] M. Verzocchi,[66] K. Vetter,[66] M. Vicenzi,[20] H. Vieira de Souza,[161] C. Vignoli,[75] C. Vilela,[127] E. Villa,[35] S. Viola,[105] B. Viren,[20] A. P. Vizcaya Hernandez,[44] Q. Vuong,[175] A. V. Waldron,[172] M. Wallbank,[40] J. Walsh,[139] T. Walton,[66] H. Wang,[25] J. Wang,[186] L. Wang,[126] M. H. L. S. Wang,[66] X. Wang,[66] Y. Wang,[25] K. Warburton,[109] D. Warner,[44] L. Warsame,[88] M. O. Wascko,[156,178] D. Waters,[203] A. Watson,[16] K. Wawrowska,[178,191] A. Weber,[134,66] C. M. Weber,[143] M. Weber,[14] H. Wei,[130] A. Weinstein,[109] S. Westerdale,[26] M. Wetstein,[109] K. Whalen,[178] A. White,[197] A. White,[214] L. H. Whitehead,[29] D. Whittington,[192] J. Wilhlemi,[214] M. J. Wilking,[143] A. Wilkinson,[203] C. Wilkinson,[126] F. Wilson,[178] R. J. Wilson,[44] P. Winter,[8] W. Wisniewski,[184] J. Wolcott,[200] J. Wolfs,[175] T. Wongjirad,[200] A. Wood,[81] K. Wood,[126] E. Worcester,[20] M. Worcester,[20] M. Wospakrik,[66] K. Wresilo,[29] C. Wret,[175] S. Wu,[143] W. Wu,[66] W. Wu,[24] M. Wurm,[134] J. Wyenberg,[53] Y. Xiao,[24] I. Xiotidis,[88] B. Yaeggy,[40] N. Yahlali,[84] E. Yandel,[27] J. Yang,[80] K. Yang,[156] T. Yang,[66] A. Yankelevich,[24] N. Yershov,[†] K. Yonehara,[66] T. Young,[148] B. Yu,[20] H. Yu,[20] J. Yu,[197] Y. Yu,[87] W. Yuan,[57] R. Zaki,[216] J. Zalesak,[49] L. Zambelli,[51] B. Zamorano,[73] A. Zani,[99] O. Zapata,[6] L. Zazueta,[192] G. P. Zeller,[66] J. Zennamo,[66] K. Zeug,[213] C. Zhang,[20] S. Zhang,[91] M. Zhao,[20] E. Zhivun,[20] E. D. Zimmerman,[43] S. Zucchelli,[92,17] J. Zuklin,[49] V. Zutshi,[149] and R. Zwaska[66]

(DUNE Collaboration)

[1]*Abilene Christian University, Abilene, Texas 79601, USA*
[2]*University of Albany, SUNY, Albany, New York 12222, USA*
[3]*University of Amsterdam, NL-1098 XG Amsterdam, The Netherlands*
[4]*Antalya Bilim University, 07190 Döşemealtı/Antalya, Turkey*
[5]*University of Antananarivo, Antananarivo 101, Madagascar*
[6]*University of Antioquia, Medellín, Colombia*
[7]*Universidad Antonio Nariño, Bogotá, Colombia*
[8]*Argonne National Laboratory, Argonne, Illinois 60439, USA*
[9]*University of Arizona, Tucson, Arizona 85721, USA*
[10]*Universidad Nacional de Asunción, San Lorenzo, Paraguay*
[11]*University of Athens, Zografou GR 157 84, Greece*
[12]*Universidad del Atlántico, Puerto Colombia, Atlántico, Colombia*
[13]*Augustana University, Sioux Falls, South Dakota 57197, USA*
[14]*University of Bern, CH-3012 Bern, Switzerland*
[15]*Beykent University, Istanbul, Turkey*
[16]*University of Birmingham, Birmingham B15 2TT, United Kingdom*
[17]*Università di Bologna, 40127 Bologna, Italy*
[18]*Boston University, Boston, Massachusetts 02215, USA*
[19]*University of Bristol, Bristol BS8 1TL, United Kingdom*
[20]*Brookhaven National Laboratory, Upton, New York 11973, USA*
[21]*University of Bucharest, Bucharest, Romania*
[22]*University of California Berkeley, Berkeley, California 94720, USA*
[23]*University of California Davis, Davis, California 95616, USA*

[24]University of California Irvine, Irvine, California 92697, USA
[25]University of California Los Angeles, Los Angeles, California 90095, USA
[26]University of California Riverside, Riverside California 92521, USA
[27]University of California Santa Barbara, Santa Barbara, California 93106, USA
[28]California Institute of Technology, Pasadena, California 91125, USA
[29]University of Cambridge, Cambridge CB3 0HE, United Kingdom
[30]Universidade Estadual de Campinas, Campinas-SP, 13083-970, Brazil
[31]Università di Catania, 2-95131 Catania, Italy
[32]Universidad Católica del Norte, Antofagasta, Chile
[33]Centro Brasileiro de Pesquisas Físicas, Rio de Janeiro, RJ 22290-180, Brazil
[34]IRFU, CEA, Université Paris-Saclay, F-91191 Gif-sur-Yvette, France
[35]CERN, The European Organization for Nuclear Research, 1211 Meyrin, Switzerland
[36]Institute of Particle and Nuclear Physics of the Faculty of Mathematics and Physics of the Charles University, 180 00 Prague 8, Czech Republic
[37]University of Chicago, Chicago, Illinois 60637, USA
[38]Chung-Ang University, Seoul 06974, South Korea
[39]CIEMAT, Centro de Investigaciones Energéticas, Medioambientales y Tecnológicas, E-28040 Madrid, Spain
[40]University of Cincinnati, Cincinnati, Ohio 45221, USA
[41]Centro de Investigación y de Estudios Avanzados del Instituto Politécnico Nacional (Cinvestav), Mexico City, Mexico
[42]Universidad de Colima, Colima, Mexico
[43]University of Colorado Boulder, Boulder, Colorado 80309, USA
[44]Colorado State University, Fort Collins, Colorado 80523, USA
[45]Columbia University, New York, New York 10027, USA
[46]Comisión Nacional de Investigación y Desarrollo Aeroespacial, Lima, Peru
[47]Centro de Tecnologia da Informacao Renato Archer, Amarais-Campinas, SP-CEP 13069-901
[48]Central University of South Bihar, Gaya, 824236, India
[49]Institute of Physics, Czech Academy of Sciences, 182 00 Prague 8, Czech Republic
[50]Czech Technical University, 115 19 Prague 1, Czech Republic
[51]Laboratoire d'Annecy de Physique des Particules, Université Savoie Mont Blanc, CNRS, LAPP-IN2P3, 74000 Annecy, France
[52]Daresbury Laboratory, Cheshire WA4 4AD, United Kingdom
[53]Dordt University, Sioux Center, Iowa 51250, USA
[54]Drexel University, Philadelphia, Pennsylvania 19104, USA
[55]Duke University, Durham, North Carolina 27708, USA
[56]Durham University, Durham DH1 3LE, United Kingdom
[57]University of Edinburgh, Edinburgh EH8 9YL, United Kingdom
[58]Universidad EIA, Envigado, Antioquia, Colombia
[59]Eötvös Loránd University, 1053 Budapest, Hungary
[60]Erciyes University, Kayseri, Turkey
[61]Faculdade de Ciências da Universidade de Lisboa-FCUL, 1749-016 Lisboa, Portugal
[62]Universidade Federal de Alfenas, Poços de Caldas-MG, 37715-400, Brazil
[63]Universidade Federal de Goias, Goiania, GO 74690-900, Brazil
[64]Universidade Federal do ABC, Santo André-SP, 09210-580, Brazil
[65]Universidade Federal do Rio de Janeiro, Rio de Janeiro-RJ, 21941-901, Brazil
[66]Fermi National Accelerator Laboratory, Batavia, Illinois 60510, USA
[67]University of Ferrara, Ferrara, Italy
[68]University of Florida, Gainesville, Florida 32611-8440, USA
[69]Florida State University, Tallahassee, Florida, 32306 USA
[70]Fluminense Federal University, 9 Icaraí Niterói-RJ, 24220-900, Brazil
[71]Università degli Studi di Genova, Genova, Italy
[72]Georgian Technical University, Tbilisi, Georgia
[73]University of Granada & CAFPE, 18002 Granada, Spain
[74]Gran Sasso Science Institute, L'Aquila, Italy
[75]Laboratori Nazionali del Gran Sasso, L'Aquila AQ, Italy
[76]University Grenoble Alpes, CNRS, Grenoble INP, LPSC-IN2P3, 38000 Grenoble, France
[77]Universidad de Guanajuato, Guanajuato, C.P. 37000, Mexico
[78]Harish-Chandra Research Institute, Jhunsi, Allahabad 211 019, India
[79]University of Hawaii, Honolulu, Hawaii 96822, USA

[80]*Hong Kong University of Science and Technology, Kowloon, Hong Kong, China*
[81]*University of Houston, Houston, Texas 77204, USA*
[82]*University of Hyderabad, Gachibowli, Hyderabad-500 046, India*
[83]*Idaho State University, Pocatello, Idaho 83209, USA*
[84]*Instituto de Física Corpuscular, CSIC and Universitat de València, 46980 Paterna, Valencia, Spain*
[85]*Instituto Galego de Física de Altas Enerxías, University of Santiago de Compostela,*
Santiago de Compostela, 15782, Spain
[86]*Indian Institute of Technology Kanpur, Uttar Pradesh 208016, India*
[87]*Illinois Institute of Technology, Chicago, Illinois 60616, USA*
[88]*Imperial College of Science, Technology and Medicine, London SW7 2BZ, United Kingdom*
[89]*Indian Institute of Technology Guwahati, Guwahati, 781 039, India*
[90]*Indian Institute of Technology Hyderabad, Hyderabad 502285, India*
[91]*Indiana University, Bloomington, Indiana 47405, USA*
[92]*Istituto Nazionale di Fisica Nucleare Sezione di Bologna, 40127 Bologna BO, Italy*
[93]*Istituto Nazionale di Fisica Nucleare Sezione di Catania, I-95123 Catania, Italy*
[94]*Istituto Nazionale di Fisica Nucleare Sezione di Ferrara, I-44122 Ferrara, Italy*
[95]*Istituto Nazionale di Fisica Nucleare Laboratori Nazionali di Frascati, Frascati, Roma, Italy*
[96]*Istituto Nazionale di Fisica Nucleare Sezione di Genova, 16146 Genova GE, Italy*
[97]*Istituto Nazionale di Fisica Nucleare Sezione di Lecce, 73100-Lecce, Italy*
[98]*Istituto Nazionale di Fisica Nucleare Sezione di Milano Bicocca, 3-I-20126 Milano, Italy*
[99]*Istituto Nazionale di Fisica Nucleare Sezione di Milano, 20133 Milano, Italy*
[100]*Istituto Nazionale di Fisica Nucleare Sezione di Napoli, I-80126 Napoli, Italy*
[101]*Istituto Nazionale di Fisica Nucleare Sezione di Padova, 35131 Padova, Italy*
[102]*Istituto Nazionale di Fisica Nucleare Sezione di Pavia, I-27100 Pavia, Italy*
[103]*Istituto Nazionale di Fisica Nucleare Laboratori Nazionali di Pisa, Pisa PI, Italy*
[104]*Istituto Nazionale di Fisica Nucleare Sezione di Roma, 00185 Roma RM, Italy*
[105]*Istituto Nazionale di Fisica Nucleare Laboratori Nazionali del Sud, 95123 Catania, Italy*
[106]*Universidad Nacional de Ingeniería, Lima 25, Perú*
[107]*University of Insubria, Via Ravasi, 2, 21100 Varese VA, Italy*
[108]*University of Iowa, Iowa City, Iowa 52242, USA*
[109]*Iowa State University, Ames, Iowa 50011, USA*
[110]*Institut de Physique des 2 Infinis de Lyon, 69622 Villeurbanne, France*
[111]*Institute for Research in Fundamental Sciences, Tehran, Iran*
[112]*Instituto Superior Técnico-IST, Universidade de Lisboa, 1049-001 Lisboa, Portugal*
[113]*Instituto Tecnológico de Aeronáutica, Sao Jose dos Campos, Brazil*
[114]*Iwate University, Morioka, Iwate 020-8551, Japan*
[115]*Jackson State University, Jackson, Mississippi 39217, USA*
[116]*Jawaharlal Nehru University, New Delhi 110067, India*
[117]*Jeonbuk National University, Jeonrabuk-do 54896, South Korea*
[118]*Jyväskylä University, FI-40014 Jyväskylä, Finland*
[119]*Kansas State University, Manhattan, Kansas 66506, USA*
[120]*Kavli Institute for the Physics and Mathematics of the Universe, Kashiwa, Chiba 277-8583, Japan*
[121]*High Energy Accelerator Research Organization (KEK), Ibaraki, 305-0801, Japan*
[122]*Korea Institute of Science and Technology Information, Daejeon, 34141, South Korea*
[123]*National Institute of Technology, Kure College, Hiroshima, 737-8506, Japan*
[124]*Taras Shevchenko National University of Kyiv, 01601 Kyiv, Ukraine*
[125]*Lancaster University, Lancaster LA1 4YB, United Kingdom*
[126]*Lawrence Berkeley National Laboratory, Berkeley, California 94720, USA*
[127]*Laboratório de Instrumentação e Física Experimental de Partículas,*
1649-003 Lisboa and 3004-516 Coimbra, Portugal
[128]*University of Liverpool, L69 7ZE, Liverpool, United Kingdom*
[129]*Los Alamos National Laboratory, Los Alamos, New Mexico 87545, USA*
[130]*Louisiana State University, Baton Rouge, Louisiana 70803, USA*
[131]*Laboratoire de Physique des Deux Infinis Bordeaux-IN2P3, F-33175 Gradignan, Bordeaux, France*
[132]*University of Lucknow, Uttar Pradesh 226007, India*
[133]*Madrid Autonoma University and IFT UAM/CSIC, 28049 Madrid, Spain*
[134]*Johannes Gutenberg-Universität Mainz, 55122 Mainz, Germany*
[135]*University of Manchester, Manchester M13 9PL, United Kingdom*

[136]*Massachusetts Institute of Technology, Cambridge, Massachusetts 02139, USA*
[137]*University of Medellín, Medellín, 050026 Colombia*
[138]*University of Michigan, Ann Arbor, Michigan 48109, USA*
[139]*Michigan State University, East Lansing, Michigan 48824, USA*
[140]*Università di Milano Bicocca, 20126 Milano, Italy*
[141]*Università degli Studi di Milano, I-20133 Milano, Italy*
[142]*University of Minnesota Duluth, Duluth, Minnesota 55812, USA*
[143]*University of Minnesota Twin Cities, Minneapolis, Minnesota 55455, USA*
[144]*University of Mississippi, University, Mississippi 38677 USA*
[145]*Università degli Studi di Napoli Federico II , 80138 Napoli NA, Italy*
[146]*Nikhef National Institute of Subatomic Physics, 1098 XG Amsterdam, Netherlands*
[147]*National Institute of Science Education and Research (NISER), Odisha 752050, India*
[148]*University of North Dakota, Grand Forks, North Dakota 58202-8357, USA*
[149]*Northern Illinois University, DeKalb, Illinois 60115, USA*
[150]*Northwestern University, Evanston, Illinois 60208, USA*
[151]*University of Notre Dame, Notre Dame, Indiana 46556, USA*
[152]*University of Novi Sad, 21102 Novi Sad, Serbia*
[153]*Occidental College, Los Angeles, California 90041*
[154]*Ohio State University, Columbus, Ohio 43210, USA*
[155]*Oregon State University, Corvallis, Oregon 97331, USA*
[156]*University of Oxford, Oxford, OX1 3RH, United Kingdom*
[157]*Pacific Northwest National Laboratory, Richland, Washington 99352, USA*
[158]*Universtà degli Studi di Padova, I-35131 Padova, Italy*
[159]*Panjab University, Chandigarh, 160014, India*
[160]*Université Paris-Saclay, CNRS/IN2P3, IJCLab, 91405 Orsay, France*
[161]*Université Paris Cité, CNRS, Astroparticule et Cosmologie, Paris, France*
[162]*University of Parma, 43121 Parma PR, Italy*
[163]*Università degli Studi di Pavia, 27100 Pavia PV, Italy*
[164]*University of Pennsylvania, Philadelphia, Pennsylvania 19104, USA*
[165]*Pennsylvania State University, University Park, Pennsylvania 16802, USA*
[166]*Physical Research Laboratory, Ahmedabad 380 009, India*
[167]*Università di Pisa, I-56127 Pisa, Italy*
[168]*University of Pittsburgh, Pittsburgh, Pennsylvania 15260, USA*
[169]*Pontificia Universidad Católica del Perú, Lima, Perú*
[170]*University of Puerto Rico, Mayaguez 00681, Puerto Rico, USA*
[171]*Punjab Agricultural University, Ludhiana 141004, India*
[172]*Queen Mary University of London, London E1 4NS, United Kingdom*
[173]*Radboud University, NL-6525 AJ Nijmegen, Netherlands*
[174]*Rice University, Houston, Texas 77005*
[175]*University of Rochester, Rochester, New York 14627, USA*
[176]*Royal Holloway College London, London, TW20 0EX, United Kingdom*
[177]*Rutgers University, Piscataway, New Jersey, 08854, USA*
[178]*STFC Rutherford Appleton Laboratory, Didcot OX11 0QX, United Kingdom*
[179]*Università del Salento, 73100 Lecce, Italy*
[180]*Universidad del Magdalena, Santa Marta, Colombia*
[181]*Sapienza University of Rome, 00185 Roma RM, Italy*
[182]*Universidad Sergio Arboleda, 11022 Bogotá, Colombia*
[183]*University of Sheffield, Sheffield S3 7RH, United Kingdom*
[184]*SLAC National Accelerator Laboratory, Menlo Park, California 94025, USA*
[185]*University of South Carolina, Columbia, South Carolina 29208, USA*
[186]*South Dakota School of Mines and Technology, Rapid City, South Dakota 57701, USA*
[187]*South Dakota State University, Brookings, South Dakota 57007, USA*
[188]*Southern Methodist University, Dallas, Texas 75275, USA*
[189]*Stony Brook University, SUNY, Stony Brook, New York 11794, USA*
[190]*Sanford Underground Research Facility, Lead, South Dakota 57754, USA*
[191]*University of Sussex, Brighton, BN1 9RH, United Kingdom*
[192]*Syracuse University, Syracuse, New York 13244, USA*
[193]*Universidade Tecnológica Federal do Paraná, Curitiba, Brazil*

[194]*Tel Aviv University, Tel Aviv-Yafo, Israel*
[195]*Texas A&M University, College Station, Texas 77840*
[196]*Texas A&M University-Corpus Christi, Corpus Christi, Texas 78412, USA*
[197]*University of Texas at Arlington, Arlington, Texas 76019, USA*
[198]*University of Texas at Austin, Austin, Texas 78712, USA*
[199]*University of Toronto, Toronto, Ontario M5S 1A1, Canada*
[200]*Tufts University, Medford, Massachusetts 02155, USA*
[201]*Universidade Federal de São Paulo, 09913-030, São Paulo, Brazil*
[202]*Ulsan National Institute of Science and Technology, Ulsan 689-798, South Korea*
[203]*University College London, London, WC1E 6BT, United Kingdom*
[204]*Universidad Nacional Mayor de San Marcos, Lima, Peru*
[205]*Valley City State University, Valley City, North Dakota 58072, USA*
[206]*University of Vigo, E- 36310 Vigo, Spain*
[207]*Virginia Tech, Blacksburg, Virginia 24060, USA*
[208]*University of Warsaw, 02-093 Warsaw, Poland*
[209]*University of Warwick, Coventry CV4 7AL, United Kingdom*
[210]*Wellesley College, Wellesley, Massachusetts 02481, USA*
[211]*Wichita State University, Wichita, Kansas 67260, USA*
[212]*William and Mary, Williamsburg, Virginia 23187, USA*
[213]*University of Wisconsin Madison, Madison, Wisconsin 53706, USA*
[214]*Yale University, New Haven, Connecticut 06520, USA*
[215]*Yerevan Institute for Theoretical Physics and Modeling, Yerevan 0036, Armenia*
[216]*York University, Toronto M3J 1P3, Canada*

[†] Affiliated with an Institute or an International Laboratory Participating within the DUNE Collaboration.